Check for updates

Received: 16 April 2022 | Revised: 31 May 2022 | Accepted: 8 June 2022

DOI: 10.1002/app.52779

RESEARCH ARTICLE

Applied Polymer SCIENCE WILEY

Preparation of highly selective PSf/ZnO/PEG400 tight ultrafiltration membrane for dyes removal

Putu Teta Prihartini Aryanti[1] | **Febrianto Adi Nugroho**[1] | **I Nyoman Widiasa**[2] | **Putu Doddy Sutrisna**[3] | **I Gede Wenten**[4,5]

[1]Chemical Engineering Department, Faculty of Engineering, Universitas Jenderal Achmad Yani, Cimahi, Indonesia

[2]Chemical Engineering Department, Universitas Diponegoro, Semarang, Indonesia

[3]Department of Chemical Engineering, Universitas Surabaya, Surabaya, Indonesia

[4]Department of Chemical Engineering, Institut Teknologi Bandung, Bandung, Indonesia

[5]Research Center for Nanosciences and Nanotechnology, Institut Teknologi Bandung, Bandung, Indonesia

Correspondence
Putu Teta Prihartini Aryanti, Chemical Engineering Department, Faculty of Engineering, Universitas Jenderal Achmad Yani, Jl. Terusan Jenderal Sudirman, Cibeber, Cimahi, 40531, Indonesia.
Email: p.teta@lecture.unjani.ac.id

Funding information
Kementerian Riset dan Teknologi/Badan Riset dan Inovasi Nasional, Grant/Award Number: 164/SP2H/LT/DRPM/2021

Abstract

Tight ultrafiltration (UF) has increasingly been developed to overcome the low selectivity of conventional UF membranes towards soluble contaminants. In this work, a tight structure of polysulfone-based (PSf) UF membrane was prepared by blending PSf with polyethylene glycol (PEG400), ZnO nanoparticle (ZnO-Np), and acetone (Ac) in dimethylacetamide (DMAc). The influences of Ac/DMAc ratio (1: 15 to 1:25) and PEG400 concentration (0–25 wt%) on the binodal curve of the polymer solution, characteristics, and performances of the UF membrane were studied. The membrane performances were investigated by observing the permeate flux and dye rejection during real textile wastewater treatment. The binodal curves are close to the polymer line, which means that rapid demixing occurred after the casted solution was immersed in the coagulation bath. Based on FTIR analysis, PEG400 and ZnO-Np were partially entrapped in the UF membrane structure. Over 90% of color removal at a permeate flux of 72 $L.m^{-2}.h^{-1}$ could be achieved when the Ac/DMAC ratio was 1:12. The tight-UF membrane removed TDS and Naphthol AS by 74.5% and 92.8%, respectively. Since the experimental result showed a high contaminants removal, the tight-UF could be used as clean technology to produce clean water for water reuse purposes at low energy requirements.

KEYWORDS

dyes removal, reuse water, tight structure, ultrafiltration

1 | INTRODUCTION

Ultrafiltration (UF) membrane has fascinated outstanding research due to its ability to molecular separation at low energy consumption.[1–4] With a pore size between 0.01 and 0.1 μm or 10 and 100 nm, the UF membrane excellently removes suspended solids, colloidal matter, proteins, bacteria, and even viruses from a water source.[5,6] Due to its advantages, this technology is widely used as a single unit for surface water treatment, which significantly reduces energy requirements and operational costs. However, low rejection of soluble contaminants, such as dyes and humic substances, becomes a limitation when it is used for water or wastewater with a high content of contaminants.[7,8] Therefore, some modifications in UF membranes are studied to improve their selectivity while maintaining high productivity. Recently, tight ultrafiltration (tight-UF) membrane has gained more attention due to its higher selectivity than conventional UF. The tight UF membrane is characterized by its pore size between 300 and 5000 Da or 2–10 nm, which lies between conventional UF and nanofiltration (NF) pore size range.[9,10] Several studies have been

 © 2022 Wiley Periodicals LLC.

focused on preparing,[11,12] improving,[13,14] or investigating the tight UF performances during its application,[15,16] both polymeric- and ceramic-based membranes.

The tight UF membranes have been used for various separation processes, such as dyes removal in textile wastewater,[17,18] humic substances removal,[19] or recovery of active compounds from several types of natural products.[20] They have shown their excellent in removing dyes, such as congo red, direct red 23, direct red 80, and reactive blue up to 99.8% and salts, such as NaCl and Na_2SO_4, up to 98%.[16,17] In peat water treatment, the tight UF membrane provided humic substances rejection up to 80% and demonstrated a stable flux up to 150 min of operating time.[19,21,22] Meanwhile, in whey wastewater treatment, the tight UF membrane, with a surface pore size of ~10 nm, reduced COD, BOD, and TSS up to 99%.[15] When the wastewater contains a high concentration of organic and inorganic contaminants, a pretreatment unit is needed prior to the tight UF membrane to prevent rapid fouling formation in the membrane system.[23] The polymeric-based tight UF membranes are generally operated between 1 and 4 bars,[24,25] while tight ceramic membranes are operated up to 8 bars.[17] The relatively high fabrication cost of ceramic membranes and the difficulty in controlling pores during the manufacture of ceramic membranes limit the development and application of ceramic-based tight UF membranes. Therefore, polymeric membranes are still widely used, particularly in water treatment.[26]

The polymeric tight UF membranes are generally prepared by several methods, including crosslinking,[11] interfacial polymerization,[27] and phase inversion methods.[28–31] Among these methods, phase inversion is considered as a simple method. This method involves separating homogenous (one phase) membrane solutions into two phases, namely rich polymer and lean polymer.[32] In the phase inversion method, the final membrane structure is intensely affected by the thermodynamic property of the membrane solution, which is generally analyzed by considering the binodal curve in a ternary diagram.[33] The binodal curve defines the phase transformation boundaries of the membrane solution. A further change in concentration of elements across the binodal curve causes liquid–liquid demixing (or phase separation).[34] The phase separation could be generated by non-solvent induced phase separation method (NIPS).

In the NIPS method, the binodal curve is influenced by the interaction between polymer, solvent, and non-solvent components.[35,36] There are many factors affecting the phase separation in membrane solution, including polymer concentration, type and composition of solvent and non-solvent, and operating condition.[37–39] High interaction between components in the membrane system results in delay phase separation, which produces a membrane with an open porous surface and sponge-like structure below the surface layer.[40] Otherwise, the low interaction contributes to rapid phase separation, generating a finger-like structure membrane with a fine porous surface layer. The high concentration of polymer leads to gel formation with a number of solvents entrapped inside the polymer matrix.[41] The high viscosity of the polymer solution may inhibit pore growth, either in or below the surface layer.[42] The presence of fillers, including polymers (such as polyethylene glycol/PEG, polyvinilpirollidone/PVP, or zwitterionic) and inorganic particles (such as titanium dioxide/TiO_2, silver/Ag, zinc oxide/ZnO, carbon nanotube /CNT, or graphene), reduces the interaction between polymer and solvent.[43–45] Therefore, solvent and non-solvent exchange could be accelerated, which induced faster phase separation and solidification of the membrane structure. Han[28] fabricated polyamideimide (PAI)/sulfonated polyphenylenesulfone (sPPSU) tight UF membrane by single-step spinning process. The mixture of two polymers resulted in delayed phase separation and resulted in a thicker sponge-like structure. The presence of hydrophilic PPSU improved the hydrophilicity of polyamideimide (PAI) membrane compared to the unmodified membrane. The tight UF membrane had a pore size of 1000–2000 Da, which provided permeate flux of 82.5–117.6 $L.m^{-2}.h^{-1}.bar^{-1}$, dye rejection of 93.2%–99.9%, and salt rejection of 90%.

The properties of solvent also affect the morphology and characteristics of the resulting UF membrane.[46] The high solubility of solvents with polymer, such as dimethylacetamide (DMAc), dimethylformamide (DMF), or N-methyl pyrrolidone (NMP), are preferable in a porous membrane preparation. The high solubility solvent induces instantaneously demixing, where the skin layer of the membrane is immediately formed after the membrane solution is immersed in the coagulation bath.[46,47] The addition of co-solvent into the membrane solution may change the liquid–liquid demixing behavior as well as the resulting membrane structure. Some studies added volatile solvents into the polymer solution, such as tetrahydrofuran (THF),[48] ethanol,[49] and acetone.[50] The volatile solvent generates rapid vitrification of polymer on the top layer of the membrane. As a result, a few pores and defects are formed in the membrane skin layer.[51] Aryanti[22] prepared a polysulfone (PSf)-based tight UF membrane by blending the polymer with PEG400 and acetone. The tight UF membrane reduced humic substances in peat water by 80% at a permeate flux of 126 $L.m^{-2}.h^{-1}$. Up to the present time, only a few studies focused on tight UF membrane preparation by phase inversion method, particularly the concentration ratio of

the solvent mixture. Therefore, further research is continuously conducted to improve selectivity while maintaining high permeability.

In this paper, a tight structure of UF membranes was prepared by blending polymers (PSf and PEG400) with ZnO nanoparticles (ZnO-Np) at various ratios of acetone and DMAC as the solvent. The PEG400 was used as a pore-performer during the membrane preparation. It has been reported that the presence of PEG could improve the porosity and hydrophilicity of the resulted membrane.[52] Meanwhile, ZnO is one of the metallic oxide particles, which provides antibacterial activity, non-toxic, and low-cost (Zhao et al., 2018). In addition, the presence of functional groups, such as —OH, —SO3H, and —COOH causes the ZnO possesses strong hydrophilicity.[53] The focus in this study was laid on the influence of solvent ratio on the characteristics and performances of the resulted membranes. The performances of the resulting tight UF membrane were investigated during the real textile wastewater treatment, which was obtained from one of the textile industries in Cimahi, Indonesia. Produced membranes from this research resulted in high dye rejection efficiency showing the potential of tight UF membranes for textile dyes treatment.

2 | MATERIAL AND METHOD

2.1 | Materials

Polysulfone/PSf (UDEL-P3500 LCD MB7) was supplied by Solvay Advanced Polymers with a molecular weight of 77.000–83.000 $g.mol^{-1}$ and a specific gravity of 1.24. N-dimethyl acetamide (DMAc, purity of 99.9%) was supplied by Shanghai Jingsan Jingwei Chemical Co. Ltd. and used without further purification. Meanwhile, ZnO-Np (20–30 nm), PEG400, and acetone (Ac) were purchased from local suppliers. Naphthol AS (3-hydroxy-2-naphthoic acid anilide, $C_{17}H_{13}NO_2$, Sigma-Aldrich) with a purity of 99% and a molecular weight (MW) of 263.29 g/mol was obtained from a local supplier. The textile wastewater was obtained from one of the textile industries in Cimahi, Indonesia, without further pre-treatment.

2.2 | Preparation of flat-sheet UF membrane

The flat-sheet UF membrane was prepared by immersion precipitation, referring to our previous study.[22] The preparation step is shown in Figure 1a. PSf, PEG400, and ZnO-Np were blended with a solvent containing DMAc and acetone. The concentration of PSf was 18 and 20 wt%, while the concentration of PEG400 varied from 0 to 25 wt%. The ZnO-Np was added into the membrane solution at a concentration of 1 wt% from the total weight of polymers. Meanwhile, the ratio of Ac/DMAc was varied by 1:15, 1:20, and 1:25. The membrane solution was stirred for 24 h until homogenous. In the first step, ZnO-Np was added to DMAc and then stirred to disperse the particles homogeneously in the solvent. Subsequently, PEG400 was added gradually to improve the dispersion of ZnO-Np,[54] followed by the addition of PSf, PEG, and acetone. The polymer solution was further stirred until homogeneous and stopped until all the bubbles in the solution disappeared. The homogenous membrane solution was cast on the glass plate with a membrane thickness of 150 μm. The casted membrane solution was immediately immersed in a coagulation bath filled with demineralized water at room temperature (±28°C). After 10 min, the UF membrane was immersed in other coagulation baths for 24 h to ensure all solvent evaporated from the membrane structure. The resulted UF membrane was cut into a circle and placed in a membrane module for permeate flux test.

2.3 | Determination of permeate flux and solute rejection of the UF membrane

The determination of permeate flux refers to our previous study,[55] as shown in Figure 1b. The UF membrane system was operated in a cross-flow mode under a transmembrane pressure (or TMP) of 15 psig and an average cross-flow velocity (CFV) of 0.5 $m.s^{-1}$. The ultrafiltration of textile wastewater was conducted for 120 min (2 h). The permeate flux was measured every 20 min. The permeate flux was calculated by the following equation:

$$J = {}^{V}/_{A.t} \tag{1}$$

where J, V, A, and t were permeate flux (in $L.m^{-2}.h^{-1}$), permeate volume (in L), effective membrane area (in m^2), and permeation time (in hour), respectively.

Meanwhile, the solute rejection was determined by measuring color, TDS, and naphthol rejection. The Naphthol AS is commonly used in most textile industries as a coupling agent for azo dyes. The solute rejection was calculated by the following equation:

$$R = \left(1 - {}^{C_p}/_{C_f}\right) \tag{2}$$

where Cp and Cf are the concentration of solutes in permeate (purified water) and feed solution (textile wastewater). The color of the textile wastewater and permeate was measured using a color water checker (Hanna instrument, HI

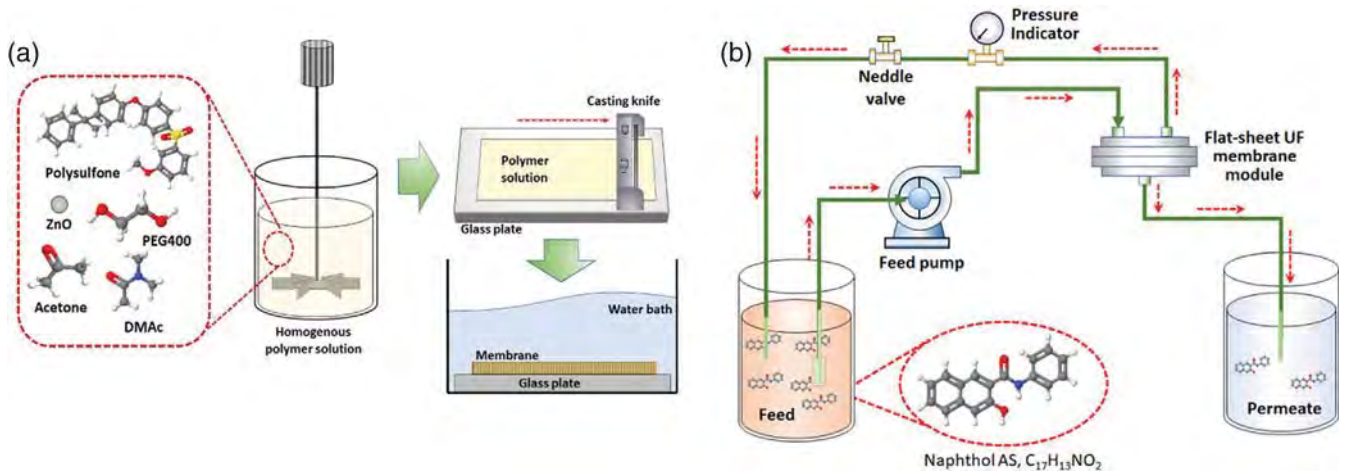

FIGURE 1 Schematic of experimental set-up for: (a) membrane preparation and (b) flux measurement of the UF membranes [Color figure can be viewed at wileyonlinelibrary.com]

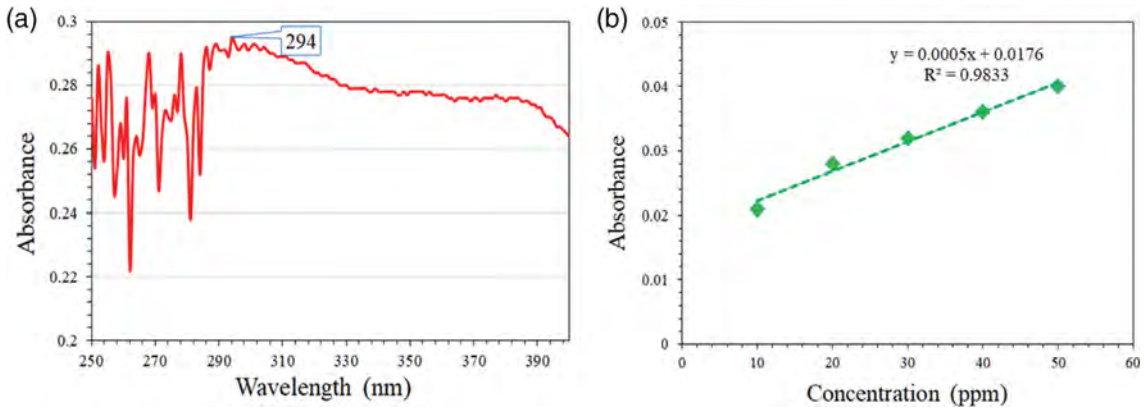

FIGURE 2 (a) Wavelength at maximum absorbance and (b) absorbance values at various concentrations of Naphthol AS. [Color figure can be viewed at wileyonlinelibrary.com]

727 (0–500 PCU). Meanwhile, TDS concentration was measured using TDS meter (HM Digital, Taiwan). Besides of color, selectivity of the resulting UF membrane was defined by Naphthol AS rejection. The concentration of Naphthol AS was determined using a UV–vis spectrophotometer (M501 Scanning Single Beam, CamSpec). The calibration curve was developed by fitting the absorbance against Naphthol AS solution at the wavelength at maximum absorbance. It was found that the maximum absorbance was detected at a wavelength of 294 nm. The absorbance value of maximum wavelength and concentrations of Naphthol AS was presented in Figures 2a,b.

2.3.1 | Morphology and psycho-chemical properties characterization

The morphology of resulted UF membranes was characterized by scanning electron microscopy (SEM) using a JEOL JSM-6510A microscope at an accelerating voltage of 10 kV. The sample of the resulting membranes was frozen by liquid nitrogen and then immediately fractured to obtain the cross-section side. The samples were sputter-coated with gold using a sputter coater before the observation.

FTIR spectrophotometer (DRS-8000, Shimadzu, Japan) was used to examine the chemical changes in the resulting UF membranes within the range of 4000–400 cm^{-1}. Prior to analysis, the UF membrane samples were dried for at least 48 h in a desiccator to remove water in the membrane structure.

2.3.2 | Cloud point test method

The cloud point test was conducted to determine the binodal curve in the ternary diagram.[56] A given concentration of PSf, PEG400, acetone, and DMAc was

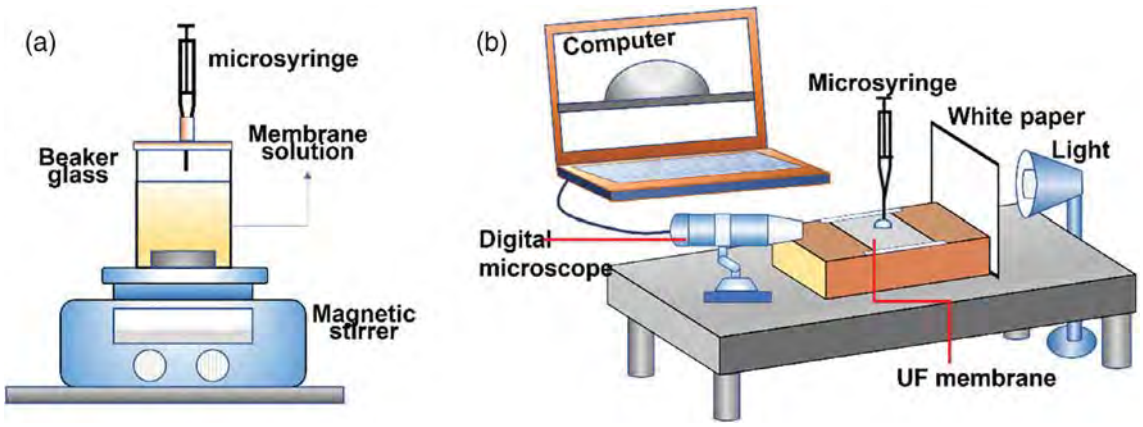

FIGURE 3 Schematic of experimental set-up for: (a) cloud point test, and (b) contact angle measurement [Color figure can be viewed at wileyonlinelibrary.com]

blended in a sealed beaker glass at 300 rpm (Magnetic Stirrer DLAB, MS-H280-PRO) and room temperature. Then, the homogenous polymer solution was slowly titrated with deionized water. When the local gelation of the polymer occurred, the polymer solution was continuously stirred to re-dissolve the polymer. The water was added to the polymer solution until the polymer solution became permanently turbid, which is known as the cloud point. The binodal curve was plotted as the concentration of non-solvent (water), solvent (DMAc and acetone), and polymers (PSf and PEG400) in weight percent (wt%). The schematic of the cloud point test apparatus is presented in Figure 3a. The influence of PSf concentration (10–20 wt%) on the thermodynamic property of the membrane solution was investigated without the presence of PEG400. Meanwhile, the effect of PEG400 concentration on the solution properties was studied at a constant PSf concentration of 20 wt%.

2.3.3 | Contact angle measurement

Contact angles of demineralized water on the membrane surface were determined via a sessile drop technique and then observed using a USB digital microscope (Figure 3b). The 3 μl of a water droplet was placed on the membrane surface using a microsyringe (Hamilton, max. Water capacity of 50 μl). Five measurements were taken at different locations on the membrane surface to define the average contact angle value. The angle between the water droplet and the membrane surface was analyzed using the ImageJ software (version v1.53n).

2.3.4 | Determination of UF membrane porosity

The porosity (ε, in %) of the UF membranes was determined by the gravimetry method, as indicated below:

$$\varepsilon_0(\%) = \frac{(W_w - W_d)/\rho_i}{\left(\frac{W_w - W_d}{\rho_i}\right) + \left(\frac{W_d}{\rho_p}\right)} \times 100 \quad (3)$$

where W_w and W_d are the weight of wet and dry UF membranes (in g). Meanwhile, ρ_i and ρ_p are the density of water (0.998 g.cm^{-3}) and PSf (1.23 g.cm^{-3}). Before being weighed, the flat-sheet UF membrane sample was immersed in demineralized water for at least 12 h to ensure that all the UF membrane pores were filled with water. The excess water on the membrane surface was gently cleaned using a napkin, and then they were weighed. Afterward, the wet membrane was dried for 48 h in a vacuum desiccator to evaporate all water from the membrane structure and then weighed.

3 | RESULTS AND DISCUSSIONS

3.1 | Thermodynamic analysis of the UF membrane solution

Thermodynamic properties of the membrane solution were analyzed by cloud point test to obtain binodal curve in ternary diagram. The influence of PSf and PEG400 concentration and solvent ratio on thermodynamic of membrane solution was investigated. The experimental results of the cloud point tests are presented in

(a)

PSF (wt.%)	PEG400 (wt.%)	Water (wt.%)		
		1:15	1:20	1:25
10	0	0.349	0.349	0.616
12	0	0.349	0.299	0.309
14	0	0.309	0.279	0.329
16	0	0.299	0.299	0.349
20	0	0.309	0.319	0.269

(b)

PSF (wt.%)	PEG400 (wt.%)	Water (wt.%)
20	0	0.309
20	10	0.249
20	15	0.200
20	20	0.180
20	25	0.120

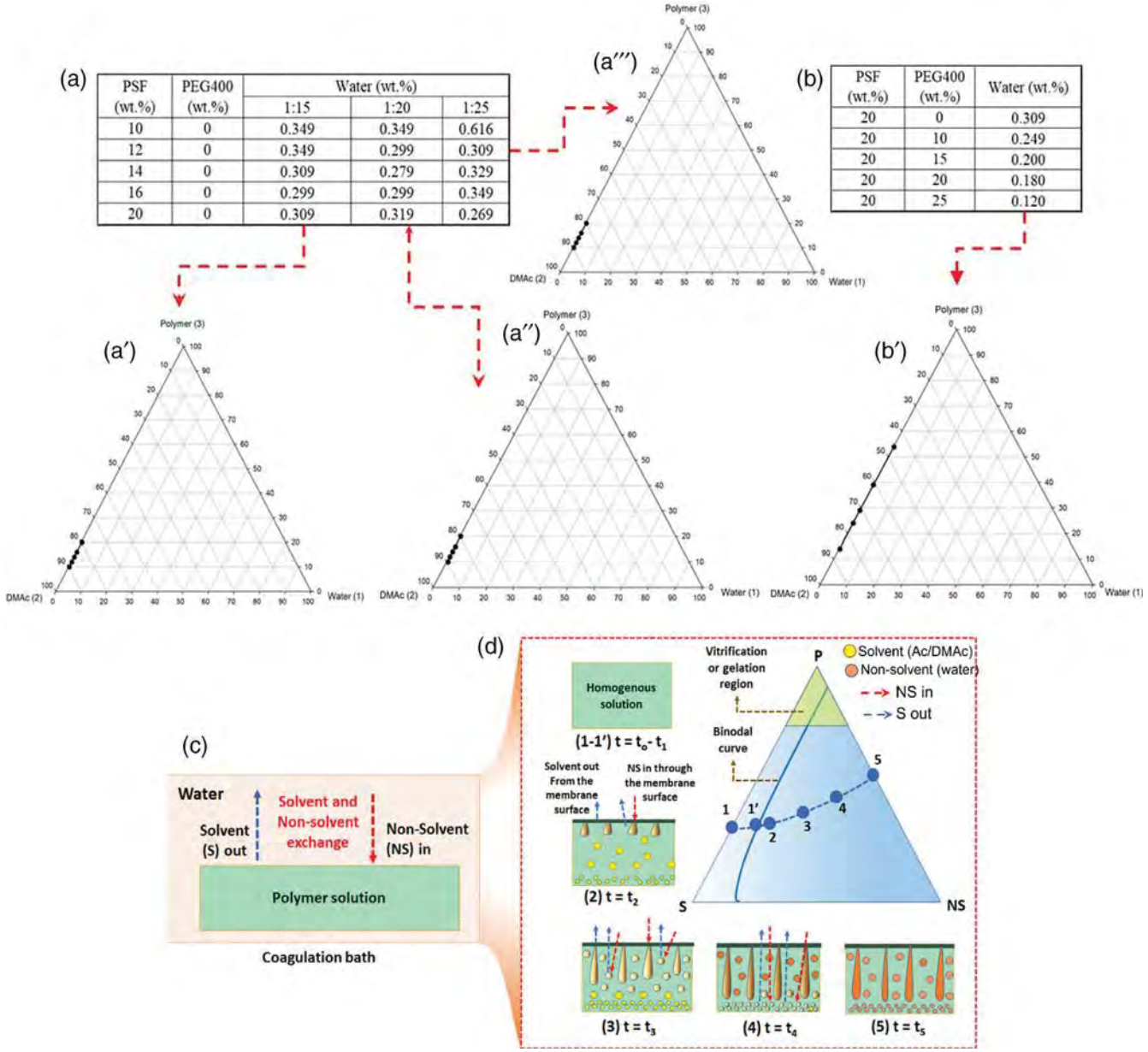

FIGURE 4 Binodal composition at: (a) PSf/PEG400/Water at ac/DMAc ratio: (a′) 1:15, (a″) 1:20, (a‴) 1:25; (b) /PEG400/Water at ac/DMAC 1:15; (c) schematic of solvent/non-solvent exchange in coagulation bath; and (d) schematic of membrane pore formation during immersion in coagulation bath [Color figure can be viewed at wileyonlinelibrary.com]

Figures 4a,b. It is shown that the binodal curves are tremendously closed to the PSf and solvent (Ac/DMAc) lines. The polymer precipitation rapidly occurred when it was contacted with the water in the coagulation bath. Based on the experimental results, there was no significant change in the amount of water required to bring the homogeneous solution cloudy at the PSf concentration of 10–20 wt%. The same results were observed when the solvent concentration ratio (Ac/DMAc) was changed. The minimum concentration of water required to induce phase separation in the PSf/Ac/DMAc system at Ac/DMAc ratio of 1:15 was between 0.299 and 0.349 wt%. While at Ac/DMAc ratios of 1:20 and 1:25, the minimum water required was between 0.279 to 0.349 wt% and 0.329 to 0.616 wt%, respectively. The results show that the amount of water needed for phase separation was increased with the decrease in polymer and acetone concentration. The change of equilibrium boundary (binodal curve) in different concentrations of PEG400 is shown in Figure 4b. Dissimilar to solvent ratio, the addition of PEG400 into the membrane solution brought the binodal curve to the top of the polymer line. When the PEG400 concentration was increased from 0 to 25 wt% at a constant PSf concentration at 20 wt%, the concentration of

water in the equilibrium curve decreased from 0.309 to 0.120 wt% (or by 61%).

It has been previously studied that the binodal curve or equilibrium boundary of the membrane solution is strongly affected by the interaction between the components, namely non-solvent (NS), solvent (S), and polymer (P).[41] The interaction of components in membrane solution is commonly notified as g_{12} for NS and S, g_{13} for NS and P, and g_{23} for S and P.[35,47] These interactions influence the mass transfer rate between S and NS during the immersion process in a coagulation bath (Figure 4c). A small value of g_{12} implies a stronger polar interaction between S and NS.[57] The NS may quickly enter the membrane solution to form finger-like structures in the resulting membrane (Figure 4d). The DMAc and acetone provide high solubility with water. Their interaction parameters with water have been reported in the literature.[57–59] High solubility in water and less affinity with PSf lead to an increase in the precipitation rate of the membrane solution. The presence of acetone (volatile solvent) induces rapid vitrification of the rich polymer in the top layer of the membrane. As a result, a defect-free or tight structure of UF membrane could be formed. In addition, the presence of volatile solvent (acetone) and non-volatile solvent (DMAc) in the membrane solution affects the evaporation rate and skin formation during the immersion precipitation process. Since the thickness and pore structure are related to the evaporation rate of solvent, the solvent ratio (Ac/DMAc) becomes a key parameter to produce thin and tight structure of the resulting UF membrane.

The addition of PEG400 into the membrane solution reduced the amount of water to reach the equilibrium condition. The presence of additives in the membrane solution reduced the miscibility of membrane solution, particularly interaction between PSf and DMAc (g_{23}). The insolubility is increased along with the increase of PEG400 concentration, and thus, less volume of water is required for the phase separation phenomenon in membrane solution.[41] In addition, the hydrophilic nature of PEG400 enhances the inflow rate of water into the membrane solution, which leads to the formation of a finger-like structure. All solvents will be eliminated at the end of the membrane structure formation, where the membrane pores are only filled with water (point 5, in Figure 4d).

3.2 | The influence of solvent ratio on the morphology of the resulting UF membranes

The influence of solvent ratio on the resulting UF membrane structure was analyzed through Scanning electron microscopy (SEM) of a cross-section of the membranes at a magnification of 500× (Figure 5). In this research, ZnO-Np was added by 1 wt% of the total weight of the polymer. It has been reported that the addition of ZnO-Np may improve the features of a membrane in terms of permeability and antifouling.[60] As shown in Figure 5, all of UF membranes had a dense retentive layer on the top-side (skin) layer of the membrane and finger-like cavities in the sub-layer below the skin layer. When the UF membrane was prepared by blending 18 wt% of PSf with ZnO-Np only (without PEG400) at Ac/DMAc ratio of 1:15, finger-like structures were formed along with the membrane thickness (Figure 5a). The acetone (as volatile solvent) might rapidly evaporate after the membrane solution was cast on the glass plate before the membrane was immersed in the coagulation bath. The rapid evaporation of acetone initiated the polymer-rich on the top of the membrane solution to undergo rapid vitrification and formed a thick skin layer. The solid surface layer hindered the evaporation of solvent to leave the membrane solution. As a result, the membrane solution had a longer time to separate into two phases (rich and lean polymer). The lean polymer phase had time to grow and form larger cavities before they solidified.[46] The decrease of the exchange rate between solvent and non-solvent during the immersion process enhanced polymer lean phase growth and coalescence.

Consequently, longer or larger finger-like pores are formed in the sub-layer of the membrane.[61] The large finger-like structure could also be attributed to the presence of hydrophilic ZnO-Np, which enhanced the water inflow to the membrane solution. When 20 wt.% of PEG400 was added into the solution (Figure 5b), the growth of membrane pore was inhibited due to higher viscosity of the membrane solution. The solvent tended to form new nuclei and then grew to create a new membrane pore.

Further increase of PEG400 concentration in the membrane solution, coalescence between membrane pores due to high concentration of water might occur, and therefore, a larger size of finger-like structure was formed (Figure 5c). The finger-like pore could be reduced by the increase of polymer concentration (Figure 5d). Higher concentration of polymer (PSf) decreased the membrane pore growth due to the change in viscosity as well as the degree of polymer chain entanglement.[51,62] When the acetone concentration was reduced, the skin layer of the UF membrane became thinner (Figure 5e-f).

Figures 5g until 5 k show the influence of PEG400 and Ac/DMAc ratio on the resulting pore structure at a constant PSf (20 wt%) and ZnO-Np concentration. Similar to the PSf concentration of 18 wt%, the change in concentration of PEG400 and ratio of Ac/DMAc influenced

the growth of membrane pore. The presence of PEG400 induced large pore formation in the membrane structure. At PSf concentration of 20 wt% and Ac/DMAc ratio of 1:15 with the addition of ZnO-Np only (Figure 5j), the UF membrane had smaller pores with some large cavities in the middle-layer and sponge-like structure in the

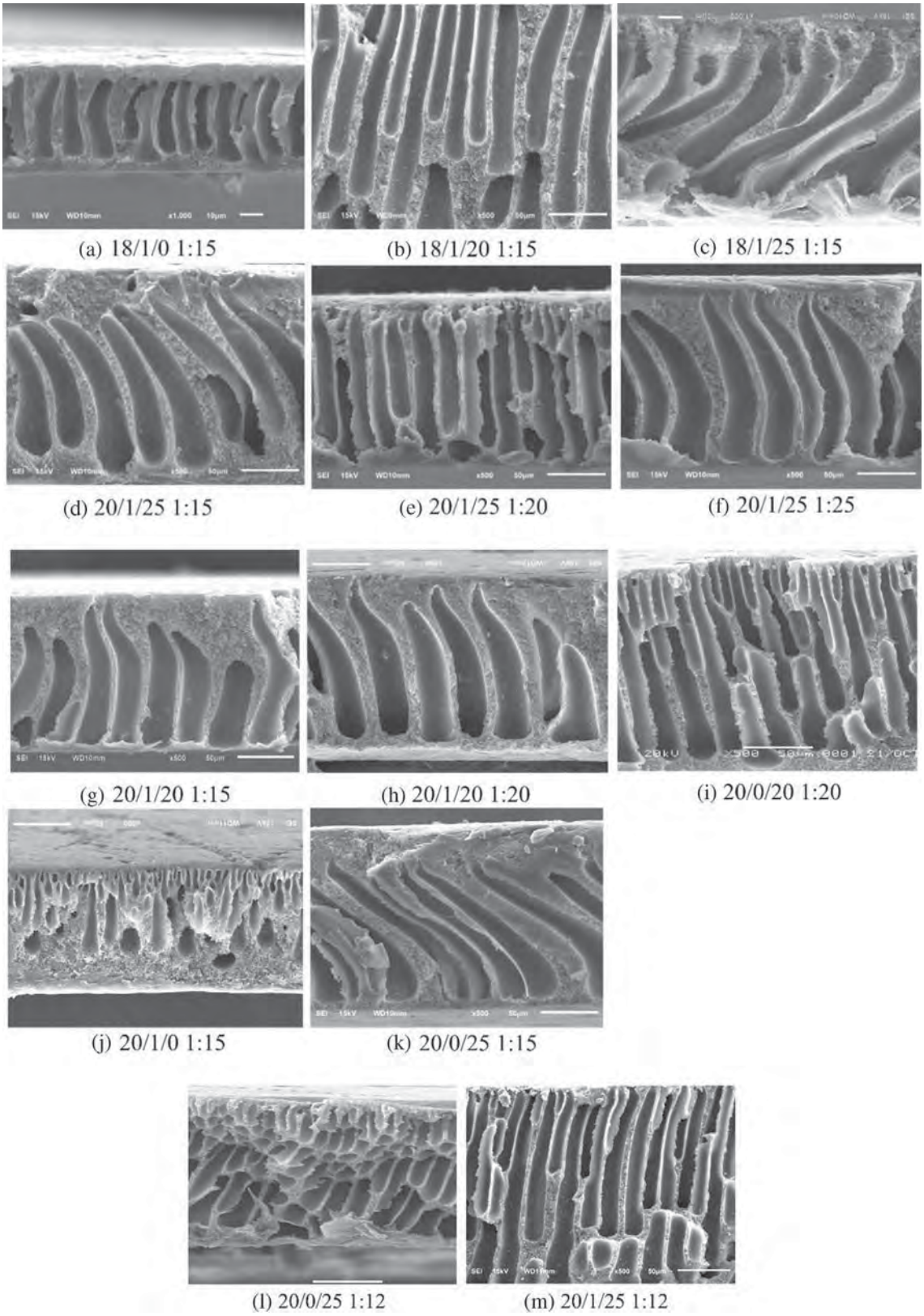

FIGURE 5 Scanning electron microscopy (SEM) of the cross-section UF membranes at different concentrations of PSf, PEG400, and solvent ratio (Ac/DMAc)

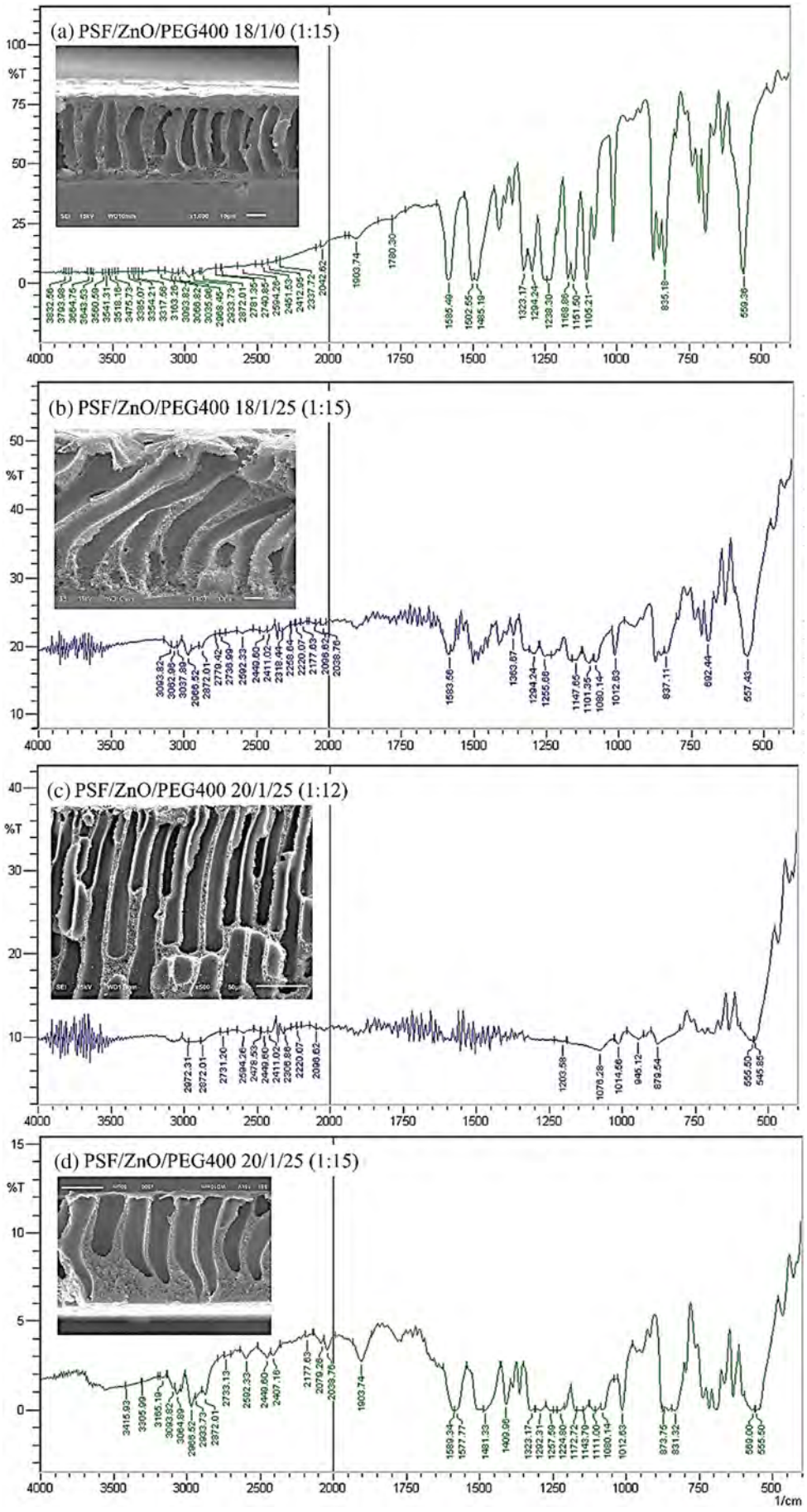

FIGURE 6 FTIR–ATR spectra of the UF membranes [Color figure can be viewed at wileyonlinelibrary.com]

bottom layer. The result showed that a high concentration of PSf and acetone, without the presence of PEG400, reduced the membrane pore significantly. The fast evaporation rate of acetone caused the polymer phase to coagulate and quickly produce a tight structure in the skin layer. At the bottom layer, the remaining solvent tended to form more new nuclei than to grow since it is hindered by the viscosity of the solution. This result showed that the presence of PEG400 had a significant effect on the final membrane pore formed in the membrane structure. Figure 5l,m showed the final membrane structures when the UF membranes were prepared at an Ac/DMAc ratio of 1:12. A smaller ratio of Ac/DMAc resulted in thicker and tighter skin layers with slimmer finger-like structures in the sub-layer of the membranes.

3.3 | Chemical properties of the resulted tight-UF membranes

The chemical analysis of the UF membranes at various polymers and Ac/DMAc ratios are presented in Figure 6. Absorptions of PSf in the membrane structure were identified by O═S═O stretch (1000–1300 cm^{-1}),[63] aromatic ring stretch (C═C—C) (1485–1585 cm^{-1}), and C—H stretch in the aromatic ring (3130–3070 cm^{-1})[64] (Figure 6a). The —OH groups on PEG400 were identified by the presence of broad absorption peaks at a wavelength between 3000 and 3600 cm^{-1}.[65] When PEG400 was added to the membrane solution (Figure 6b-d), a broad peak was observed in the range of 3250 to 4000 cm^{-1}. The peaks between 3250 and 3650 cm^{-1} indicated the hydrogen bond. Meanwhile, peaks between 3550 and 3670 cm^{-1} indicated compounds containing an oxygen-related group in PEG400. Another peak up to 4000 cm^{-1} identified single bond area.[64] The absorption band identifies the presence of ZnO-Np was detected at a wavelength between 442 to 576 cm^{-1}.[66,67] The presence of functional groups of additives (PEG400 and ZnO-Np) in the membrane structure implied that the additives were not leached out into the non-solvent. The solidification of surface layer inhibited the additives from leaving the membrane structure during the immersion precipitation process. Therefore, partial hydrophilic additives remained in the membrane structure, and thus, it gave a hydrophilic property to the UF membrane.

3.4 | The influence of polymer concentration and solvent ratio on hydrophilicity and porosity of the UF membrane

The average contact angles of the resulting UF membranes at various Ac/DMAc ratios, PSf, and PEG400 concentrations are presented in Figure 7. The PSf membrane is naturally hydrophobic, but the contact angle (CA) of the neat PSf membrane is reported below 90°.[68] In this research, a high water contact angle (70° < CA < 75°) was obtained when the UF membrane was prepared at a low concentration of PEG400 (between 0 and 15 wt%) or higher concentration of PSf (20 wt%) with the addition of ZnO-Np of 1 wt% of the total weight of polymers (PEG400 and PSf). Meanwhile, the lowest contact angle (60.4°) was achieved at PSf/ZnO/PEG400 of 20/1/25 and Ac/DMAc of 1:25. A similar result resulted at PSf/ZnO/PEG400 of 18/1/25 and Ac/DMAc of 1:25, that is, 60.6°.

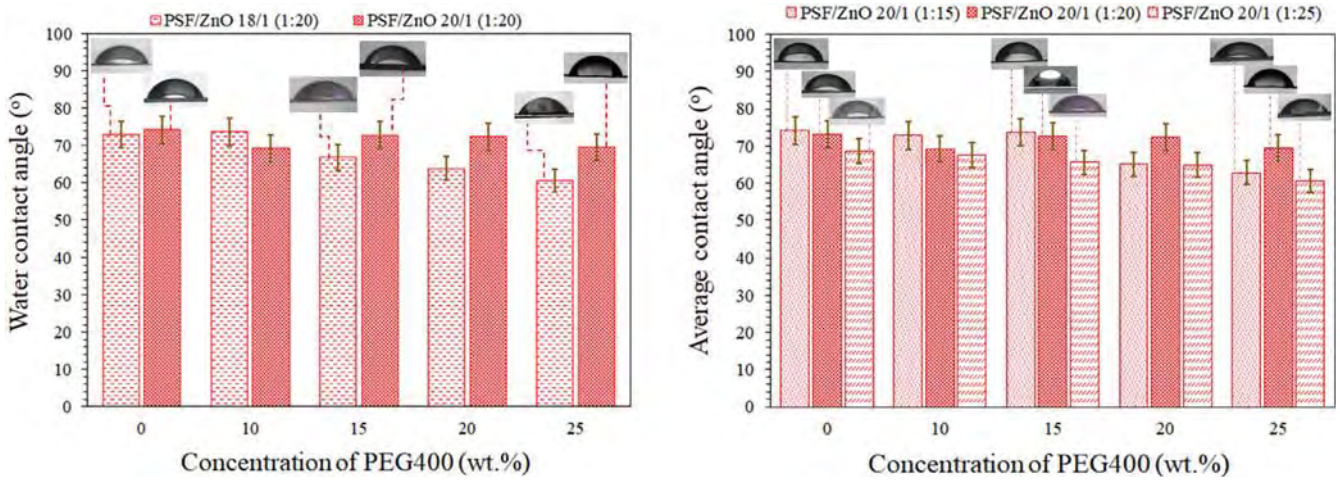

FIGURE 7 The average contact angle of the UF membranes: (a) at different PSf/PEG concentrations and (b) at different PEG/solvent ratios [Color figure can be viewed at wileyonlinelibrary.com]

A low concentration of acetone and PSf in the membrane solution reduced the amount of rich polymer in the surface membrane layer due to the shorter evaporation time of acetone. It was also suggested that the lower concentration of polymer in the membrane surface decreased the orientation of polymer chain, which contributed to larger pore size formed in the membrane surface. In addition, the presence of PEG400 and ZnO-Np, which were trapped in the membrane structure, resulted in hydrophilic characteristics and lower contact angle.

Figure 8 presents the influence of solvent ratio at various concentrations of PEG400 and PSf on the change in membrane porosity with the increase of PEG400 concentration and solvent ratio in the membrane solution. Overall, the resulting membrane porosity was between 71% and 80% when 18 and 20 wt% of PSf were blended with PEG400 from 0 to 25 wt%, ZnO-Np of 1 wt% from the total weight of polymers, and Ac/DMAc ratio from 1:15 to 1:25. A low concentration of PSf (18 wt%) resulted in a large membrane pore in the sub-layer along with the membrane thickness. The low viscosity of the membrane solution at a low concentration of PSf allowed the nuclei to grow and then form a larger pore. The UF membrane prepared by PSf of 18 wt% with the addition of ZnO-Np and Ac/DMAc ratio of 1:15 had a porosity of 76%. An elevation of PSf concentration to 20 wt% reduced the membrane porosity to 71% due to the hindrance of the pore growth by the high viscosity of the solution. The decrease of acetone concentration could increase the membrane porosity. It has been explained in Section 3.2 that a lower concentration of acetone reduced the thickness of membrane surface, and thus, the resistance of water to enter the membrane solution and evaporation of the solvent were decreased. Larger membrane porosity could be resulted by the increase of water inflow to the membrane solution. The rise of Ac/DMAc ratio from 1:15 to 1:25 at constant PSf concentration of 20 wt% enhanced the membrane porosity from 71% to 76%. At PSf concentration of 18 and PEG400 of above 15 wt%, a decrease in membrane porosity occurred when the ratio of Ac/DMAc was increased from 1:15 to 1:25. It was suggested that Ac/DMAc ratio of 1:15 produced membranes with more homogeneous pores than the ratio of 1:20 and 1:25. As previously explained that the thick membrane surface inhibited the solvent from evaporating. The presence of PEG400 (>15 wt %) was sufficient to enhance the solution viscosity and restrict the growth of pores. The remaining solvent tended to form new nuclei and grew until a specific size. Therefore, higher membrane porosity was achieved.

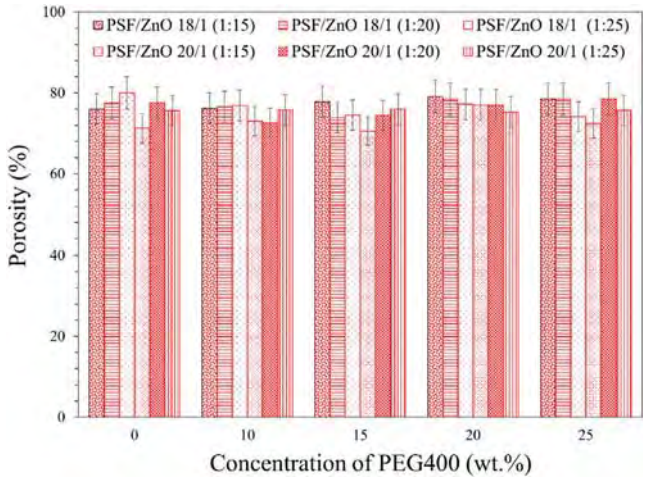

FIGURE 8 The influence of PSf/PEG concentration and solvent ratio on porosity of the UF membranes [Color figure can be viewed at wileyonlinelibrary.com]

3.5 | The influence of polymer concentration and solvent ratio on permeate flux

Profiles of permeate fluxes for the resulting membranes during textile wastewater treatment are depicted in Figure 9. The highest initial permeate flux was 134 L.m^{-2}.h^{-1} that was produced by UF membrane that was prepared by blending 20 wt% of PSf with 20 wt% of PEG400 and ZnO-Np, in a solvent (Ac/DMAc) ratio of 1:25 (membrane code: PSf/ZnO/PEG400 20/1/20 1:25). When the PEG400 concentration was increased to 25 wt % (PSf/ZnO/PEG400 20/1/25 1:25), the permeate flux was decreased to 112 L.m^{-2}.h^{-1}. The decrease of permeate flux was influenced by the morphology of the UF membrane. As shown in Figure 5a,h, the UF membrane with PEG400 of 20 wt% had a larger membrane pore size compared with the other one. It has been explained that the increase of PEG400 concentration in membrane solution may increase the viscosity of the membrane solution and suppress the growth of the membrane pores. Thus, some new nuclei were formed and then grew until a specific size. The pore size of UF membrane influenced the flux decline due to fouling during 2 h of the ultrafiltration process. The highest flux decline was achieved by the composite UF membrane PSf/ZnO/PEG400 18/1/25 with Ac/DMAc ratio of 1:25. Low concentration of PSf and acetone formed UF membrane with large pore size, as shown in Figure 5, as well as high membrane porosity. When the UF membrane was used for textile wastewater filtration, the contaminants were easily adsorbed on the membrane surface. The accumulation of contaminants on the membrane surface was raised by the increase in operating time, which enhanced the fouling resistance and hindered the solvent (water) from passing through the membrane pore. Therefore, the permeate flux was decreased.

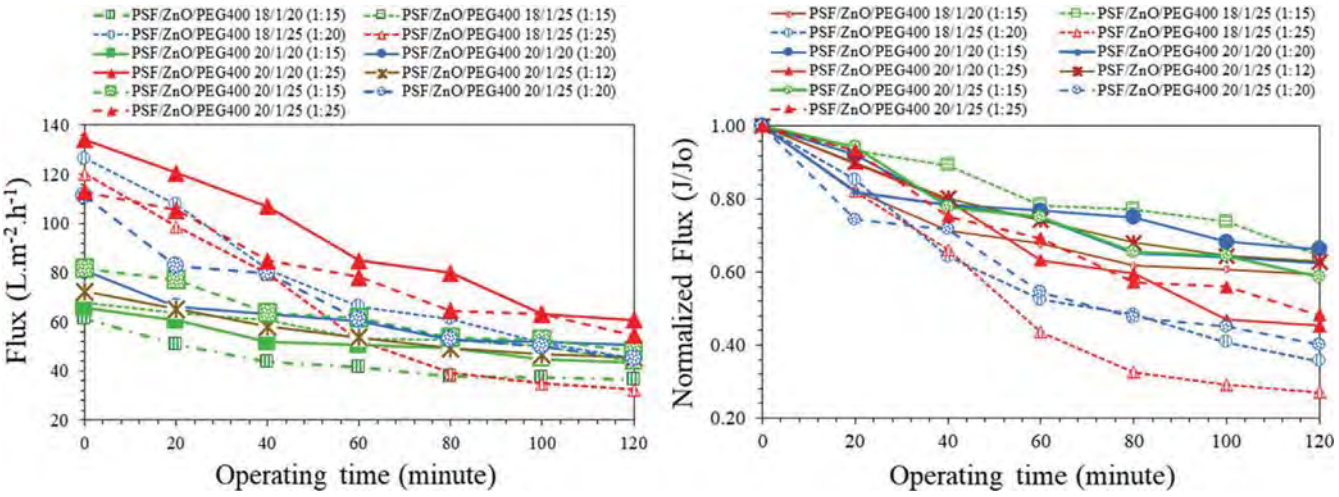

FIGURE 9 The influence of solvent ratio on (a) permeate flux and (b) normalized flux during 2 h of ultrafiltration at an operating pressure of 15 psig [Color figure can be viewed at wileyonlinelibrary.com]

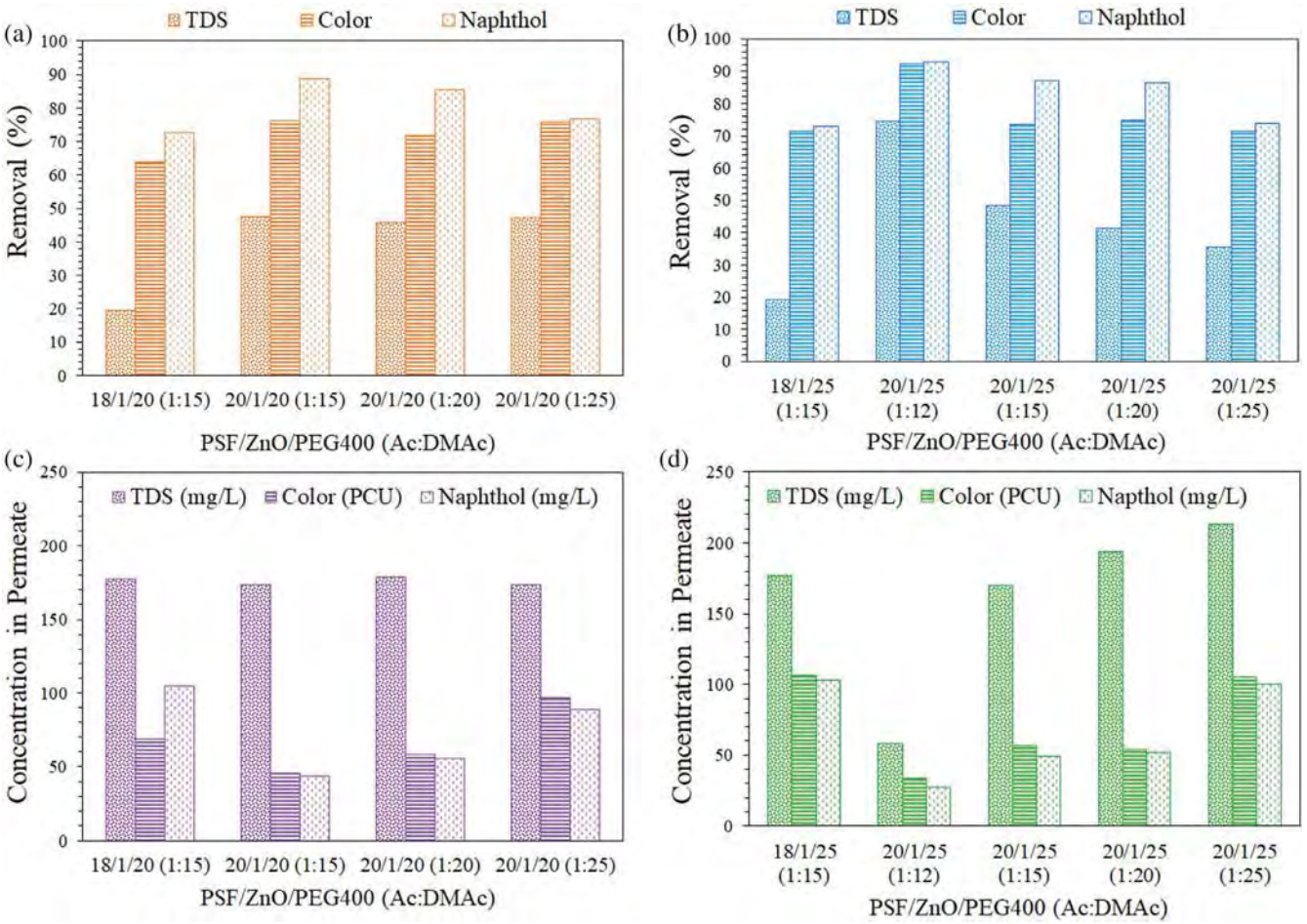

FIGURE 10 The influence of solvent ratio on removal efficiency of contaminants at different concentration of PEG400: (a, c) 20 wt%, and (b, d) 25 wt% [Color figure can be viewed at wileyonlinelibrary.com]

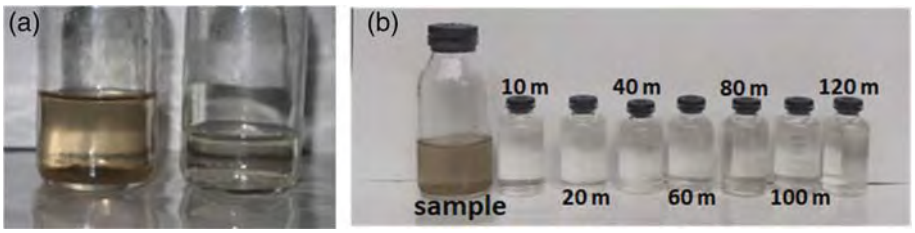

FIGURE 11 Effluent of textile wastewater treatment using tigh-UF membrane: (a) PSf/ZnO/PEG400 20/1/25 (1:15) and (b) PSf/ZnO/PEG400 20/1/25 (1:12) [Color figure can be viewed at wileyonlinelibrary.com]

TABLE 1 The comparison of tight-UF membrane performances for dyes removal with this study

Membrane materials	Membrane types	Membrane characteristics and operating conditions	Removal efficiency	Reference
PES (UH004, Microdyn-Nadir, Germany)	Hollow fiber	Membrane thickness: ~590 nm MWCO: 4700 Da Mean effective pore radius: 0.91 nm Pure water permeability: 27 $L.m^{-2}.h^{-1}.bar^{-1}$	Direct red 80, congo red and reactive blue: >98% Salt rejection	[16]
Ceramic UF membrane, coated with TiO_2 (TAMI Industries, France)	Tubular	Pure water flux: 13.61 $L.m^{-2}.h^{-2}.bar^{-1}$ MWCO: 2410 Da	Reactive dyes: >98.12% NaCl: <0.1% Na_2SO_4: <1.5%	[17]
PAEK-COOH	Flat-sheet	Dye permeation flux: 100.9 L. m-2.h-1 Pure water flux: 119.6 $L.m^{-2}.h^{-1}$ MWCO: 9260 Da	Congo red (CR) 100 ppm: 98% Salt rejection: <10%	[18]
Torlon/sPPSU	Hollow fiber	MWCO: 1000–2000 Da Mean effective pore radius: 1.0–1.3 nm Pure water permeability: 82.5–117.6 $L.m^{-2}.h^{-1}$.	Dyes removal: 93.2–99.9% Salts (Na_2SO_4 and NaCl): 92%	[28]
Ceramic (α-Al_2O_3) membrane, active layer: TiO_2/ZrO_2	Multi-tubular ceramic membrane (19 channels)	Permeability: 21.8 $L.m^{-2}.h^{-1}.bar^{-1}$ MWCO: 8800 Da Mean effective pore radius: 1.16 nm	Dyes removal (Blue KN-R, Black 5, and Red H-E7B): >98% Na_2SO_4: 14.38%	[69]
PES/SPSf/ adipic acid	Flat-sheet	Pure water flux: 72.2 $L.m^{-2}.h^{-2}.bar^{-1}$ MWCO: 7250 Da average pore size: 1.8 nm	Dyes removal: Methyl red (MR): 50.1% methyl orange (MO): 69.4% acid blue 25 (AB25): 92.6%	[70]
PSF/ZnO/PEG400 20/1/25 Ac:DMAc 1:12	Flat-sheet	Pure water flux: 72 $L.m^{-2}.h^{-1}$	Dye removal (Naphthol AS): 92.8% Salts (TDS): 74.5%	This work

Abbreviations: MWCO, molecular weight cut off; PAEK-COOH, cardo poly (arylene ether ketone)s/carboxylic acid groups; PEG400, polyethylene glycol 400; PES, polyethersulfone; sPPSU, sulfonated polyphenylenesulfone; SPSf, sulfonated polysulphone.

3.6 | The influence of polymer concentration and solvent ratio on removal efficiency of the resulting UF membrane

The influence of polymer concentration and solvent ratio on the removal efficiency of contaminants is presented in Figure 10. It shows that the removal of the contaminants could be improved by increasing the PSf concentration and solvent ratio. It was attributed to the tight structure of the skin layer of the UF membrane by the increase in polymer and acetone concentration. The highest rejections of color and Naphthol AS were achieved when

Ac/DMAC ratio of 1:12 was used in 20 wt% of PSf, 25 wt% of PEG400, and 1 wt% of ZnO-Np of the total weight of polymers. The rapid evaporation of acetone initiated the polymer-rich on the top of the membrane solution to undergo rapid vitrification and formed a thick skin layer. The tight-UF membrane removed TDS and Naphthol AS by 74.5% (from 230 to 58.57 mg.L^{-1}) and 92.8% (from 381 to 27 44 mg.L^{-1}), respectively. Meanwhile, the color of textile wastewater was reduced from 430 to 33.57 PCU or by 92.2%. The effluent of UF membrane at Ac/DMAC ratio of 1:12 resulted in a clear water product (Figure 11a). Meanwhile, the effluent for wastewater treatment by UF membrane prepared with an Ac/DMAc ratio of 1:15 resulted in effluent with a light-yellow color (Figure 11b). Since the tight-UF membrane with a ratio PSF/ZnO/PEG400 of 20/1/25 at Ac/DMAc ratio of 1:12 resulted in high removal efficiency of color and minerals in the textile wastewater, the tight-UF could be used as an alternative to produce clean water for water reuse purpose (Table 1).

4 | CONCLUSION

A tight ultrafiltration (tight-UF) membrane has been successfully prepared by blending polysulfone (PSf) with polyethylene glycol (PEG400) and ZnO nanoparticle (ZnO-Np) in a mixture of acetone and DMAc as the solvent. The concentration of ZnO-Np in the membrane solution was kept constant at 1 wt% of the total weight of polymers (PSf and PEG400) in all UF membrane preparation. The concentration of PEG400 varied from 0 to 25 wt %, while the solvent (Ac/DMAc) ratio varied from 1:15 to 1:25. The characteristics of the membrane solution and the resulting membranes were analyzed through cloud point test, SEM, FTIR, water contact angle, and porosity measurement. Meanwhile, the performances of the UF membranes were analyzed by measuring permeate flux and removal efficiency of color, TDS, and Naphthol-AS. It was found that the change in solvent ratio (Ac/DMAc) and PSf concentration did not have a significant effect on the binodal (cloud point) curve. The binodal curves were close to the polymer line, which means that rapid demixing occurred after the casted solution was immersed in the coagulation bath. The increase of PEG400 and Ac/DMAC ratio resulted in a thick and tight structures in the skin membrane layer. The final structure of the skin layer influenced the formation of pore structure in the sub-layer and bottom layer of the membrane, which impacted the membrane's porosity. Based on FTIR analysis, PEG400 and ZnO-Np were partially entrapped in the PSf membrane structure after being immersed for 24 h in a coagulation bath. The highest permeate flux of 134 L.m^{-2}.h^{-1} was achieved by the composite UF PSf/ZnO/PEG400 20/1/20 with Ac/DMAc ratio of 1:25. The UF membranes prepared by low polymer and acetone concentrations were susceptible to fouling and resulted in extremely high flux reduction (up to 73%) during the 2-h of ultrafiltration process. Over than 90% of color removal at a permeate flux of 72 L.m^{-2}.h^{-1} could be achieved when the Ac/DMAC ratio was elevated to 1:12. The rapid evaporation of acetone initiated the polymer-rich on the top of the membrane solution to undergo rapid vitrification and formed a thick skin layer. Despite the high rejection of color, the tight-UF membrane removed TDS and Naphthol AS by 74.5 and 92.8%, respectively. Hence, the tight-UF membranes from this study are potential to be applied as an alternative to produce fresh water from dyes wastewater.

AUTHOR CONTRIBUTIONS

Putu Teta Prihartini Aryanti: Conceptualization (lead); data curation (lead); formal analysis (lead); investigation (lead); methodology (lead); writing – original draft (lead); writing – review and editing (lead). **Febrianto Adi Nugroho:** Investigation (equal); writing – original draft (equal); writing – review and editing (equal). **I Nyoman Widiasa:** Conceptualization (equal); data curation (equal); formal analysis (lead); investigation (equal); methodology (equal); writing – review and editing (equal). **Putu Doddy Sutrisna:** Conceptualization (equal); data curation (equal); investigation (equal); writing – original draft (equal); writing – review and editing (equal). **I Gede Wenten:** Conceptualization (equal); methodology (equal); writing – original draft (equal); writing – review and editing (equal).

ACKNOWLEDGMENT

This research was funded by the Ministry of Education, Culture, Research, and Technology/National Research and Innovation Agency Republic of Indonesia through a program entitled: "Ministry of Education, Culture, Research and Technology 2021", with Contract No.: 164/SP2H/LT/DRPM/2021 dated 18th March 2021.

ORCID

Putu Teta Prihartini Aryanti https://orcid.org/0000-0003-0200-418X

REFERENCES

[1] A. W. Mohammad, C. Y. Ng, Y. P. Lim, G. H. Ng, *Food Bioprocess Technol.* **2012**, *5*, 1143.

[2] U. W. Siagian, K. Khoiruddin, A. K. Wardani, P. T. Aryanti, I. N. Widiasa, G. Qiu, Y. P. Ting, I. G. Wenten, *Curr. Pollut. Rep.* **2021**, *7*, 448.

[3] I. G. Wenten, P. T. P. Aryanti, K. Khoiruddin, A. N. Hakim, N. F. Himma, *J. Membr. Sci. Res.* **2016**, *2*, 78.

[4] E. Ratnaningsih, R. Reynard, K. Khoiruddin, I. G. Wenten, R. Boopathy, *Appl. Sci.* **2021**, *11*, 1078.
[5] M. Cuartucci, *Water Pract. Technol.* **2020**, *15*, 426.
[6] D. Ariono, P. T. P. Aryanti, S. Subagjo, I. G. Wenten, *AIP Conf. Proc.* **2017**, *1788*, 030048.
[7] G. Zhang, Y. Li, A. Gao, Q. Zhang, J. Cui, S. Zhao, X. Zhan, Y. Yan, *Chem. Eng. J.* **2019**, *369*, 576.
[8] W. Yu, Y. Liu, Y. Xu, R. Li, J. Chen, B.-Q. Liao, L. Shen, H. Lin, *J. Membr. Sci.* **2019**, *581*, 401.
[9] Q. Lan, C. Feng, K. Ou, Z. Wang, Y. Wang, T. Liu, *J. Membr. Sci.* **2021**, *640*, 119858.
[10] P. T. P. Aryanti, A. N. Hakim, S. Widodo, I. N. Widiasa, I. G. Wenten, *IOP Conf. Proc.: Mater. Sci. Eng.* **2018**, *395*, 012012.
[11] C. Liu, H. Mao, J. Zheng, S. Zhang, *J. Membr. Sci.* **2017**, *538*, 58.
[12] X. Huang, C. Tian, H. Qin, W. Guo, P. Gao, H. Xiao, *Ceram. Int.* **2020**, *46*, 4679.
[13] W. Ye, K. Ye, F. Lin, H. Liu, M. Jiang, J. Wang, R. Liu, J. Lin, *Chem. Eng. J.* **2020**, *379*, 122321.
[14] G. Jiang, S. Zhang, Y. Zhu, S. Gao, H. Jin, L. Luo, F. Zhang, J. Jin, *J. Mater. Chem. A* **2018**, *6*, 2927.
[15] E. S. Mansor, E. A. Ali, A. Shaban, *Chem. Eng. J.* **2021**, *407*, 127175.
[16] J. Lin, W. Ye, M.-C. Baltaru, Y. P. Tang, N. J. Bernstein, P. Gao, S. Balta, M. Vlad, A. Volodin, A. Sotto, P. Luis, A. L. Zydney, B. Van Der Bruggen, *J. Membr. Sci.* **2016**, *514*, 217.
[17] M. Jiang, K. Ye, J. Lin, X. Zhang, W. Ye, S. Zhao, B. Van Der Bruggen, *J. Membr. Sci.* **2018**, *566*, 151.
[18] C. Liu, H. Mao, J. Zheng, S. Zhang, *J. Membr. Sci.* **2017**, *530*, 1.
[19] D. Ariono, P. T. P. Aryanti, A. K. Wardani, I. G. Wenten, *Membr. Water Treat.* **2018**, *9*, 353.
[20] A. Cassano, C. Conidi, R. Ruby-Figueroa, R. Castro-Muñoz, *Int. J. Mol. Sci.* **2018**, *19*, 351.
[21] P. T. P. Aryanti, S. Subagjo, D. Ariono, I. G. Wenten, *J. Membr. Sci. Res.* **2015**, *1*, 41.
[22] P. T. P. Aryanti, A. M. Noviyani, M. F. Kurnia, D. A. Rahayu, A. Z. Nisa, *IOP Conf. Ser.: Mater. Sci. Eng.* **2018**, *288*, 012118.
[23] F. A. Nugroho, P. T. P. Aryanti, S. Nurhayati, H. M. Muna, *AIP Conf. Proc.* **2019**, *2097*, 030017.
[24] M. Jiang, K. Ye, J. Deng, J. Lin, W. Ye, S. Zhao, B. Van Der Bruggen, *Environ. Sci. Technol.* **2018**, *52*, 10698.
[25] N. A. Johari, N. Yusof, W. J. Lau, N. Abdullah, W. N. W. Salleh, J. Jaafar, F. Aziz, A. F. Ismail, *Sep. Purif. Technol.* **2021**, *270*, 118819.
[26] M. Kotobuki, Q. Gu, L. Zhang, J. Wang, *Molecules* **2021**, *26*, 3331.
[27] S. Fang, X. Shi, X. Wang, Z. Zhang, C. Yin, Z. Zhang, T. Ju, S. Xiong, Y. Wang, *J. Membr. Sci.* **2021**, *637*, 119635.
[28] G. Han, Y. Feng, T.-S. Chung, M. Weber, C. Maletzko, *Environ. Sci. Technol.* **2017**, *51*, 14254.
[29] A. Grylewicz, K. Szymański, D. Darowna, S. Mozia, *Molecules* **2021**, *26*, 2768.
[30] A. Marjani, A. T. Nakhjiri, M. Adimi, H. F. Jirandehi, S. Shirazian, *Sci. Rep.* **2020**, *10*, 1.
[31] I. Kimotho, N. M. Noah, M. Nawiri, B. Mbatia, *Adv. Polym. Technol.* **2020**, *2020*, 1.
[32] Y.-h. Tang, E. Ledieu, M.R. Cervellere, P.C. Millett, D.M. Ford and X. Qian, *J. Membr. Sci.* **2020**, *599*, 117826.
[33] C. Kahrs, M. Metze, C. Fricke, J. Schwellenbach, *J. Mol. Liq.* **2019**, *291*, 111351.
[34] C. Kahrs, J. Schwellenbach, *Polymer* **2020**, *186*, 122071.
[35] P. T. P. Aryanti, D. Ariono, A. N. Hakim, I. G. Wenten, *J. Phys. Conf. Ser.* **2018**, *1090*, 012074.
[36] K. V. Kurada, S. De, *Polym. Eng. Sci.* **2018**, *58*, 1062.
[37] S. Madaeni, L. Bakhtiari, *Polymer* **2012**, *53*, 4481.
[38] D. Sidabutar, E. Putri, N. Putri, S. Sakinah, P. Aryanti, *J. Phys. Conf. Ser.* **2020**, *1477*, 052014.
[39] F. Tibi, A. Charfi, J. Cho, J. Kim, *Process Saf. Environ. Prot.* **2020**, *141*, 190.
[40] M. Tian, J. Zhu, S. Yuan, Y. Zhang, B. Van Der Bruggen, *J. Membr. Sci.* **2021**, *630*, 119299.
[41] D. Ariono, P. T. P. Aryanti, A. N. Hakim, S. Subagjo, I. G. Wenten, *AIP Conf. Proc.* **2017**, *1840*, 090008.
[42] S. Leaper, A. Abdel-Karim, B. Faki, J. M. Luque-Alled, M. Alberto, A. Vijayaraghavan, S. M. Holmes, G. Szekely, M. I. Badawy, N. Shokri, P. Gorgojo, *J. Membr. Sci.* **2018**, *554*, 309.
[43] J. S. Taurozzi, H. Arul, V. Z. Bosak, A. F. Burban, T. C. Voice, M. L. Bruening, V. V. Tarabara, *J. Membr. Sci.* **2008**, *325*, 58.
[44] A. Abdel-Karim, J. M. Luque-Alled, S. Leaper, M. Alberto, X. Fan, A. Vijayaraghavan, T. A. Gad-Allah, A. S. El-Kalliny, G. Szekely, S. I. A. Ahmed, S. M. Holmes, P. Gorgojo, *Desalination* **2019**, *452*, 196.
[45] H. Julian, P. D. Sutrisna, A. N. Hakim, H. O. Harsono, Y. A. Hugo, I. G. Wenten, *Polym. Plast. Technol. Mater.* **2019**, *58*, 678.
[46] R. W. Baker, *Membrane technology and applications*, John Wiley & Sons, Chichester, West Sussex **2012**.
[47] M. Mulder, J. Mulder, *Basic Principles of Membrane Technology*, Kluwer Academic Publishers, Chichester, West Sussex **1996**.
[48] M. Mertens, T. Van Dyck, C. Van Goethem, A. Y. Gebreyohannes, I. F. J. Vankelecom, *J. Membr. Sci.* **2018**, *557*, 24.
[49] T. Y. Son, T. H. Ko, V. Vijayakumar, K. Kim, S. Y. Nam, *Solid State Ionics* **2020**, *344*, 115153.
[50] K. V. Kurada, A. Agarwal, S. De, *Polym. Int.* **2020**, *69*, 920.
[51] M. Aroon, A. Ismail, M. Montazer-Rahmati, T. Matsuura, *Sep. Purif. Technol.* **2010**, *72*, 194.
[52] M. Sharma, P. Mondal, A. Chakraborty, J. Kuttippurath, M. Purkait, *J. Water Process Eng.* **2019**, *30*, 100632.
[53] L. Shen, Z. Huang, Y. Liu, R. Li, Y. Xu, G. Jakaj, H. Lin, *Front. Chem.* **2020**, *8*, 224.
[54] H. Rabiee, V. Vatanpour, M. H. D. A. Farahani, H. Zarrabi, *Sep. Purif. Technol.* **2015**, *156*, 299.
[55] I. G. Wenten, K. Khoiruddin, A. K. Wardani, P. T. P. Aryanti, D. I. Astuti, A. A. I. A. S. Komaladewi, *J. Water Process. Eng.* **2020**, *34*, 101158.
[56] J.-Y. Zhou, Z.-Y. Luo, M.-J. Yin, N. Wang, Z. Qin, K.-R. Lee, Q.-F. An, *J. Membr. Sci.* **2020**, *610*, 118404.
[57] J. Y. Kim, H. K. Lee, K. J. Baik, S. C. Kim, *J. Appl. Polym. Sci.* **1997**, *65*, 2643.
[58] J. Wijmans, J. Baaij, C. Smolders, *J. Membr. Sci.* **1983**, *14*, 263.
[59] C. Tsay, A. McHugh, *J. Polym. Sci., Part B: Polym. Phys.* **1990**, *28*, 1327.

[60] P. Peechmani, M. H. D. Othman, R. Kamaludin, M. H. Puteh, J. Jaafar, M. A. Rahman, A. F. Ismail, S. H. S. A. Kadir, R. M. Illias, J. Gallagher, *J. Environ. Chem. Eng.* **2021**, *9*, 105873.
[61] Y. Ma, F. Shi, J. Ma, M. Wu, J. Zhang, C. Gao, *Desalination* **2011**, *272*, 51.
[62] T.s. Chung, E. R. Kafchinski, *J. Appl. Polym. Sci.* **1997**, *65*, 1555.
[63] H. T. V. Nguyen, T. H. A. Ngo, K. D. Do, M. N. Nguyen, N. T. T. Dang, T. T. H. Nguyen, V. Vien, T. A. Vu, *J. Chem.* **2019**, *2019*, 3164373.
[64] A. B. D. Nandiyanto, R. Oktiani, R. Ragadhita, *Indones. J. Sci. Technol.* **2019**, *4*, 97.
[65] B. Saini, M. K. Sinha, *J. Appl. Polym. Sci.* **2019**, *136*, 47163.
[66] K. Handore, S. Bhavsar, A. Horne, P. Chhattise, K. Mohite, J. Ambekar, N. Pande, V. Chabukswar, *J. Macromol. Sci., Part A* **2014**, *51*, 941.
[67] X. Li, A. Lu, H. Yang, *J. Non-Cryst. Solids* **2014**, *389*, 21.
[68] P. T. P. Aryanti, S. R. Joscarita, A. K. Wardani, S. Subagjo, D. Ariono, I. G. Wenten, *J. Eng. Technol. Sci.* **2016**, *48*, 135.
[69] X. Ma, P. Chen, M. Zhou, Z. Zhong, F. Zhang, W. Xing, *Ind. Eng. Chem. Res.* **2017**, *56*, 7070.
[70] M. Hu, S. Yang, X. Liu, R. Tao, Z. Cui, C. Matindi, W. Shi, R. Chu, X. Ma, K. Fang, M. Titus, B. B. Mamba, J. Li, *Sep. Purif. Technol.* **2021**, *266*, 118587.

How to cite this article: P. T. P. Aryanti, F. A. Nugroho, I. N. Widiasa, P. D. Sutrisna, I. G. Wenten, *J. Appl. Polym. Sci.* **2022**, e52779. https://doi.org/10.1002/app.52779

Volume 139 | Issues 33-34 2022
Included In This Print Edition:
Issue 33 (September 5, 2022)
Issue 34 (September 10, 2022)

JOURNAL OF Applied Polymer SCIENCE

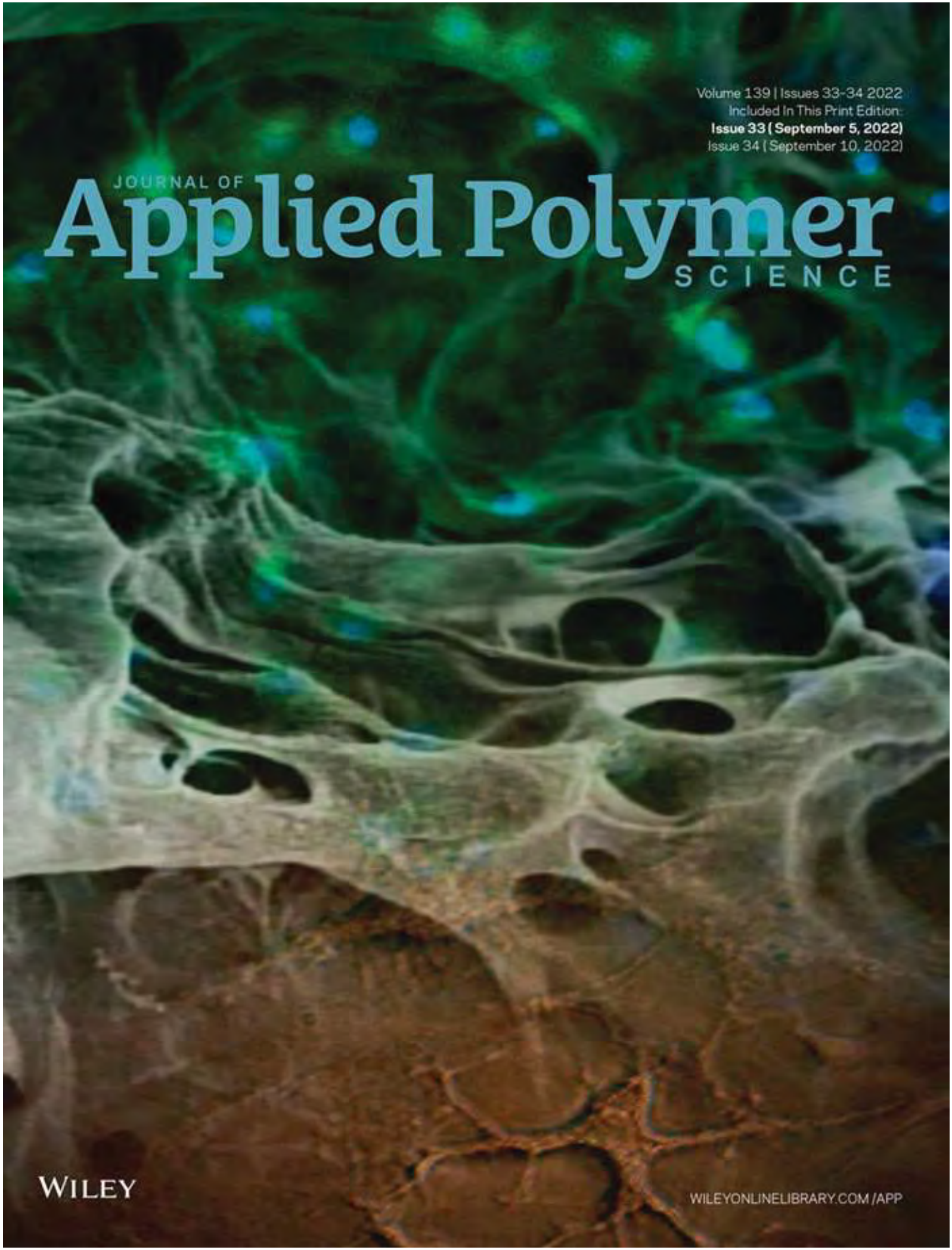

WILEY

WILEYONLINELIBRARY.COM/APP

Advertisement

JOURNAL OF Applied Polymer SCIENCE

Editorials

- *Stefano Tonzani*
  Bloggers, welcome
  J. Appl. Polym. Sci. **2013**, *130*(5), 3027.

- *Stefano Tonzani*
  Awards for the best *Journal of Applied Polymer Science* referee during 2012
  J. Appl. Polym. Sci. **2013**, *130*(2), 711-712.

- *Stefano Tonzani*
  How to make the cut
  J. Appl. Polym. Sci. **2013**, *129*(5), 2361-2362.

- *Stefano Tonzani*
  Polymers for biomedical applications
  J. Appl. Polym. Sci. **2013**, *129*(2), 527.

- *Stefano Tonzani*
  Who are you? ORCID knows the answer
  J. Appl. Polym. Sci. **2013**, *128*(5), 2585.

- *Stefano Tonzani*
  Fibers in polymer-based materials
  J. Appl. Polym. Sci. **2013**, *128*(2), 925.

- *Stefano Tonzani and Hilary J. Crichton*
  Scientific Ethics
  J. Appl. Polym. Sci. **2012**, *127*(3), 1455-1457.

- *Stefano Tonzani*
  The renaissance of polyolefins
  J. Appl. Polym. Sci. **2012**, *127*(2), 837.

- *Stefano Tonzani*
  New and improved, with a taste for applications
  J. Appl. Polym. Sci. **2012**, *127*(1), xiii-xiv.

- *Stefano Tonzani*
  Polymers in Asia-Pacific
  J. Appl. Polym. Sci. **2012**, *126*(S2), E1.

- *Stefano Tonzani*
  Polysaccharides
  J. Appl. Polym. Sci. **2012**, *126*(S1), E1.

- *Stefano Tonzani*
  Awards for the Best *Journal of Applied Polymer Science* Referees During 2011
  J. Appl. Polym. Sci. **2012**, *126*(1), 1.

- *Stefano Tonzani*
  Biopolymers and Renewably Sourced Polymers
  J. Appl. Polym. Sci. **2012**, *125*(S2), E1.

- *Stefano Tonzani*
  Polymer Composites in the Spotlight
  J. Appl. Polym. Sci. **2012**, *125*(S1), E1.

- *Stefano Tonzani*
  Polymers in Membrane Science
  J. Appl. Polym. Sci. **2012**, *124*(S1), E1.

Sign up for email alerts

Enter your email to receive alerts when new articles and issues are published.

Email address*

Enter email

Continue

Tools

Submit an Article

Browse free sample issue

Subscribe to this journal

More from this journal

Reviews
Professional Opportunities
Cover Story

Editorials
Wiley Job Network
Best of Wiley Polymer Journals eMagazine
Twitter: @WileyPolymers
Jobs

About Wiley Online Library

Privacy Policy
Terms of Use
About Cookies
Manage Cookies
Accessibility
Wiley Research DE&I Statement and Publishing Policies
Developing World Access

Help & Support

Contact Us
Training and Support
DMCA & Reporting Piracy

Opportunities

Subscription Agents
Advertisers & Corporate Partners

Connect with Wiley

The Wiley Network
Wiley Press Room

Copyright © 1999-2023 John Wiley & Sons, Inc. All rights reserved

JOURNAL OF Applied Polymer SCIENCE

Volume 139, Issue 33

September 05, 2022

‹ Previous Issue | Next Issue ›

GO TO SECTION

Export Citation(s)

COVER IMAGE

Free Access

Cover Image, Volume 139, Issue 33

Zahra Ayar, Mehdi Shafieian, Omid Sabzevari, Zahra Hassannejad

First Published: 20 July 2022

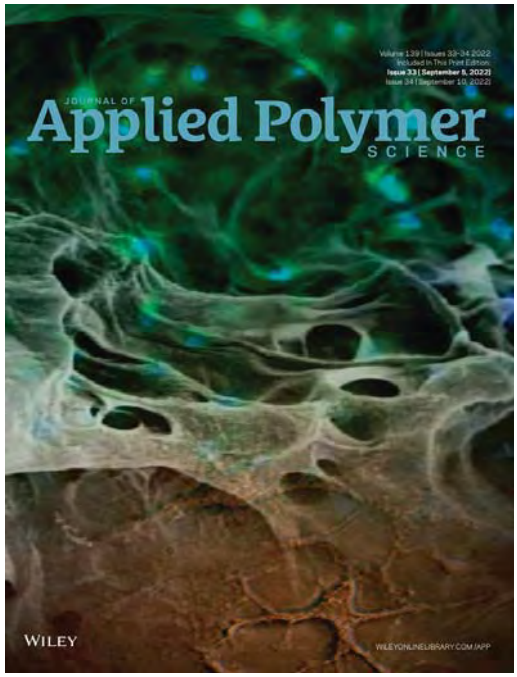

This image, taken and designed by Zahra Ayar, is a combination of SEM, fluorescent, and optical pictures of a porous alginate hydrogel that is modified using Schwann cell- and fibroblast-derived ECM. The study focused on the efficacy of cell-derived ECM modification on the differentiation potency of alginate hydrogel. This modified hydrogel provides an efficient microenvironment for differentiation of adipose-derived stem cells towards neuron-like cells. DOI: 10.1002/app.52501

Abstract | PDF | Request permissions

ISSUE INFORMATION

Free Access

Editorial Board, Aims & Scope, Table of Contents

First Published: 20 July 2022

First Page | PDF | Request permissions

RESEARCH ARTICLES

Modification of the alginate hydrogel with fibroblast- and Schwann cell-derived extracellular matrix potentiates differentiation of mesenchymal stem cells toward neuron-like cells

Zahra Ayar, Mehdi Shafieian, Omid Sabzevari, Zahra Hassannejad

First Published: 02 May 2022

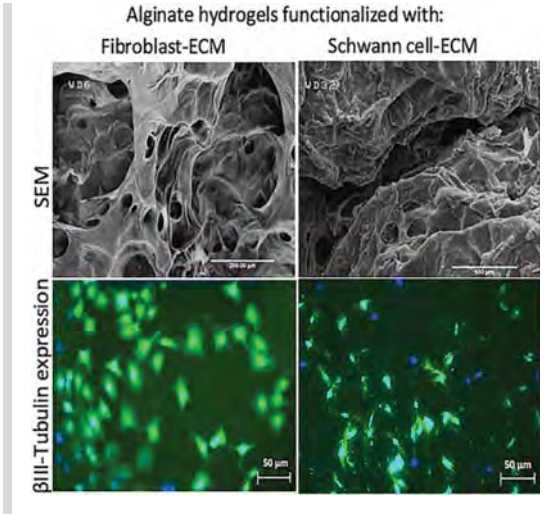

Abstract | Full text | PDF | References | Request permissions

Preparation of highly selective PSf/ZnO/PEG400 tight ultrafiltration membrane for dyes removal

Putu Teta Prihartini Aryanti, Febrianto Adi Nugroho, I Nyoman Widiasa, Putu Doddy Sutrisna, I Gede Wenten

First Published: 21 June 2022

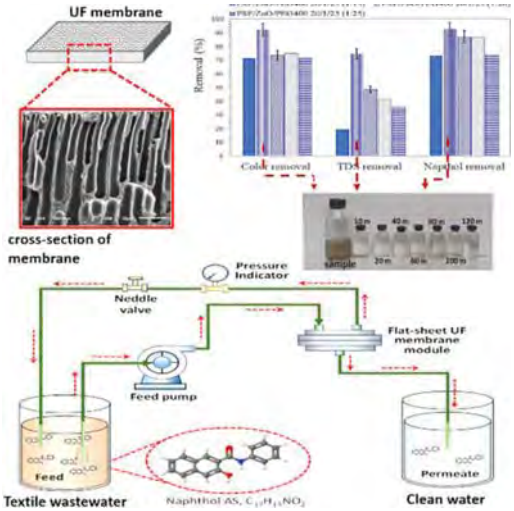

Abstract | Full text | PDF | References | Request permissions

Flexible anodic bonding for the bonding between elastomer and metal

Haocheng Zhao, Cuirong Liu, Chao Du, Ying Zhang, Zhichao Zhang, Chunping Liang, Yuling Wu

First Published: 24 June 2022

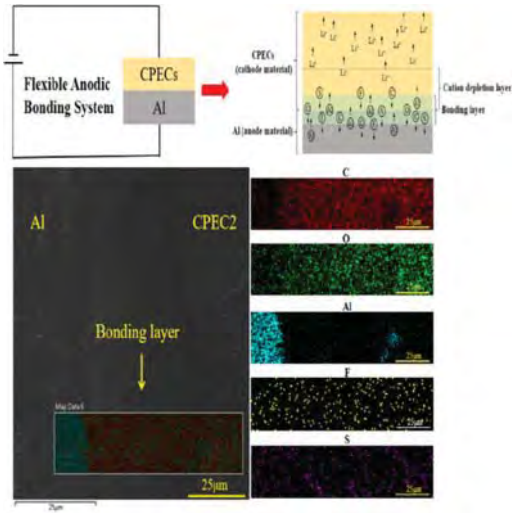

In order to improve the success rate of anodic bonding for polymer materials, the flexible anodic bonding process characterized by the dynamic intelligent electric fields, low-temperature plasma surface treatment to polymer materials, and ultrasonic-assisted pre-connection before connection has been developed. Meanwhile, a series of composite polyurethane elastomer packaging materials (CPECs) with good bonding properties are prepared and characterized. What it means that it provides a possibility for packaging of flexible MEMS device to use anodic bonding technology.

Abstract | Full text | PDF | References | Request permissions

Sustainable copper oxide/Tragacanth gum bionanocomposites with multi-purpose catalytic activities on textile

Panid Kahali, Majid Montazer, Mehdi Kamali Dolatabadi

First Published: 28 June 2022

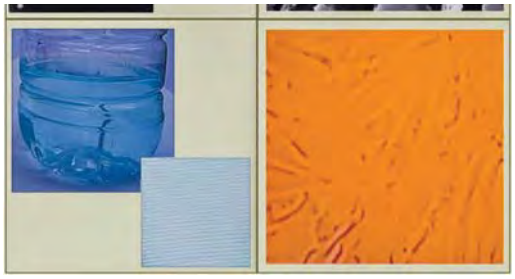

Abstract | Full text | PDF | References | Request permissions

Green composites of poly(3-hydroxybutyrate-co-3-hydroxyvalerate) and sugarcane bagasse fibers plasticized with triethyl citrate: Thermal, mechanical and morphological properties

Victor Ferrão, Giovanni Bortoloni Perin, Maria Isabel Felisberti

First Published: 24 June 2022

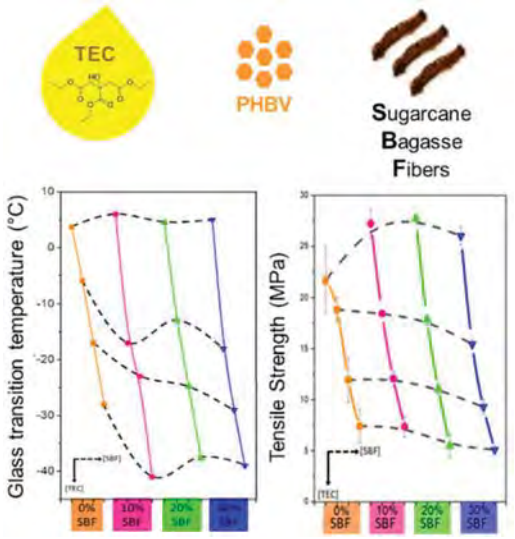

Abstract | Full text | PDF | References | Request permissions

Comparative study on the effects of water pressure on water absorption of ultra-high molecular weight polyethylene and polyformaldehyde

Song Chen, Xiangcai Bao, Zhiheng Wang, Xiangbin Rong, Xiaohong Zhang, Chao Li, Xinyu Wang, Lei Wei

First Published: 24 June 2022

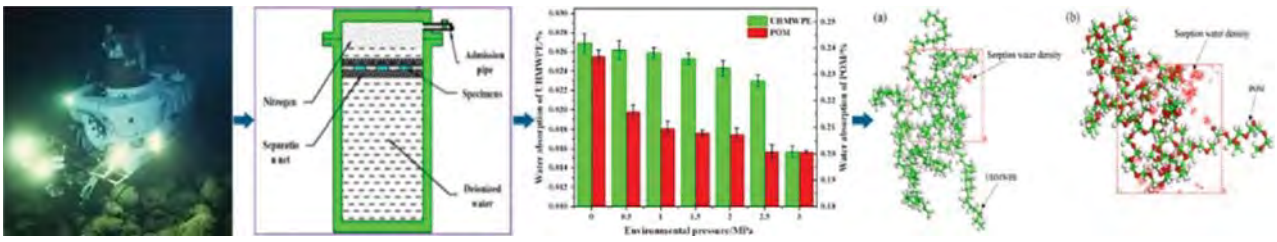

In order to explore the application of polymer materials in water environment, the water

absorption properties of ultra-high molecular weight polyethylene (UHMWPE) and polyformaldehyde (POM) were investigated through water absorption experiments and molecular dynamics simulations.

Abstract | Full text | PDF | References | Request permissions

Well-dispersed poly(ether-ether-ketone)/multi-walled carbon nanotubes nanocomposite for harsh environment applications

Zhiyuan Jiang, Zewen Zhu, Mingzhen Zhao, Hengxi Chen, Hung-Jue Sue

First Published: 23 June 2022

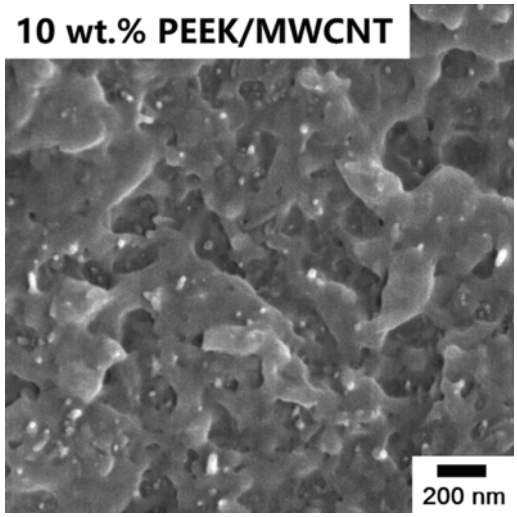

MWCNTs have been individually dispersed in PEEK matrix at a concentration of 10 wt.%, resulting in an almost doubled modulus of PEEK. This well dispersed PEEK/MWCNT nanocomposite shows highly efficient mechanical reinforcement, making it suitable for many high performance, harsh environment applications.

Abstract | Full text | PDF | References | Request permissions

Grape-clustered polyaniline grafted with carbon nanotube woven film as a flexible electrode material for supercapacitors

Bingjian Li, Shi Liu, Xixi Xu, Haicun Yang, Yinjie Zhou, Dan Yang, Yun Zhang, Jinchun Li

First Published: 23 June 2022

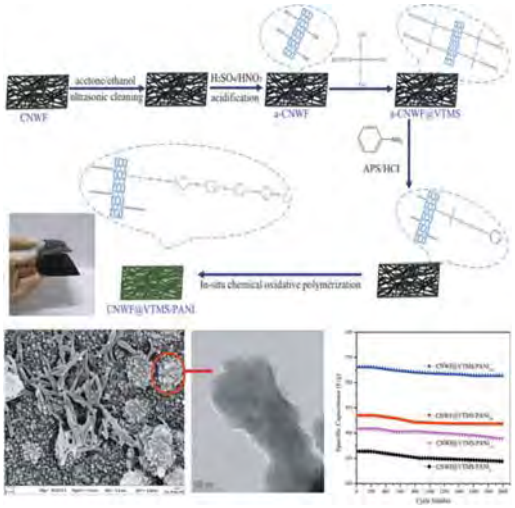

Polyaniline (PANI) with the grape-clustered structure was grafted on the surface of continuously reinforced carbon nanotube woven film (CNWF) via in-situ chemical oxidative polymerization. The strong interfacial bonding between CNWF and PANI plays an important role in improving the long-term stability of the electrochemical performance. It could be a potential application in the field of deformable supercapacitors.

Abstract | Full text | PDF | References | Request permissions

Inhibition of electrical trees degradation of crosslinked polyethylene at high temperatures by electron-buffering voltage stabilizers

Zelin Hong, Xiangrong Chen, Guangyu Zhu, Muhammad Awais, Yiwen Shi, Hanshan Zhu, Hao Li, Ashish Paramane

First Published: 24 June 2022

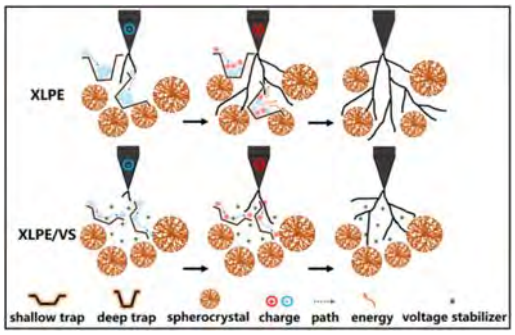

For shallow traps, negative and positive high-energy charges can easily de-trap after being injected in the AC voltage cycle. This process results in energy dissipation and reduces the probability of positive and negative charge recombination. Therefore, the molecular chain scission of the XLPE cannot occur easily. On the one hand, the combination of positive and negative charges is promoted in the case of deep traps, leading to the formation of low-density regions.

Abstract | Full text | PDF | References | Request permissions

Epoxy resin/hollow glass microspheres composite materials with low dielectric constant and excellent mechanical performance

Xiaolin Zhang, Man Liu, Yu Chen, Jiacheng He, Xuelin Wang, Jian Xie, Ziwei Li, Zhimin Chen, Yuheng Fu, Chuanxi Xiong, Shan Wang

First Published: 27 June 2022

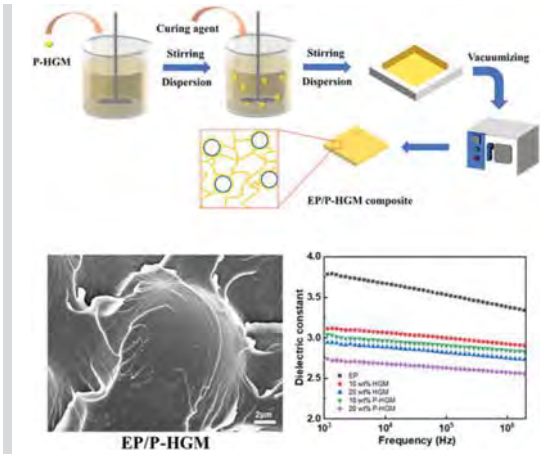

Abstract | Full text | PDF | References | Request permissions

Preparation of ethyl cellulose–glycerol tribenzoate microcapsules in CO_2/N_2-switchable hydrophilicity solvent and solvent recycling

Cunchuan Zheng, Fuchuan Liu, Ke Xu, Yang Wu, Jinyu Wang

First Published: 09 July 2022

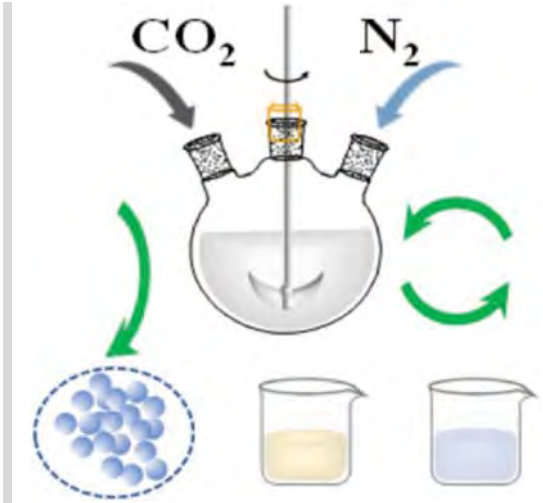

Abstract | Full text | PDF | References | Request permissions

Facile preparation of anisotropic PLA/CNT nanocomposites by hot and cold rolling processes for improving mechanical and conductive properties

An Huang, Xincheng Song, Fan Liu, Haokun Wang, Lihong Geng, Binyi Chen, Xiangfang Peng, Zhen Wang, Genlin Tian

First Published: 13 July 2022

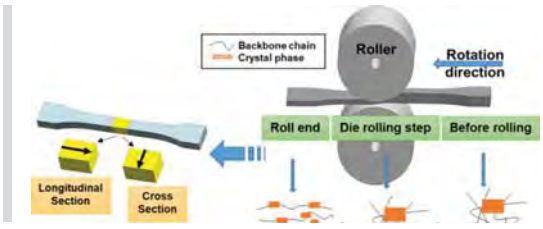

Rolling process leads to anisotropy in PLA and PLA/CNT nanocomposites

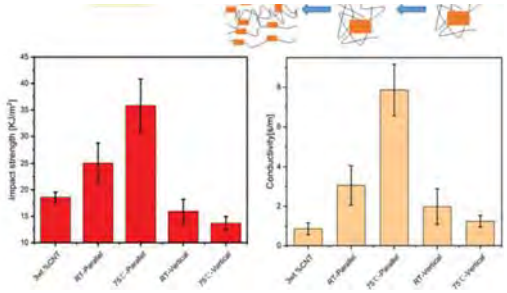

Abstract | Full text | PDF | References | Request permissions

Synthesis of dual-stimuli-responsive polyurethane shape memory nanocomposites incorporating isocyanate-functionalized Fe_3O_4 nanoparticles

Amin Babaie, Mostafa Rezaei, Donya Razzaghi, Hossein Roghani-Mamaqani

First Published: 11 July 2022

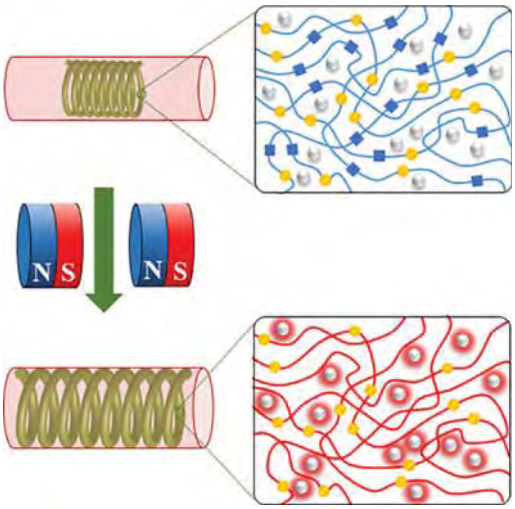

Restricted shape recovery process in the presence of an alternating magnetic field.

Abstract | Full text | PDF | References | Request permissions

Preparation of flame retardant viscose fibers by supramolecular self-assembly

Long Xie, Bo Liu, Xinhua Liu, Yueyue Lu

First Published: 11 July 2022

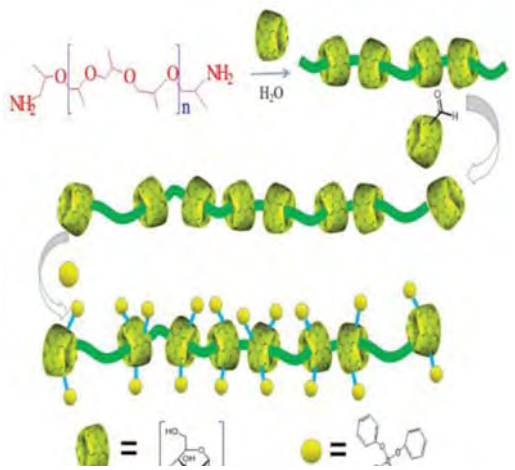

Preparation of cyclodextrin polymeric flame retardants by self-assembly technology and flame retardant modifications.

Abstract | Full text | PDF | References | Request permissions

Studies on electrolytic and doping behavior of different compounds and their combination on the electrical resistance of polypyrrole film via electrochemical polymerization

Ankur Shukla, Kushal Sen, Dipayan Das

First Published: 11 July 2022

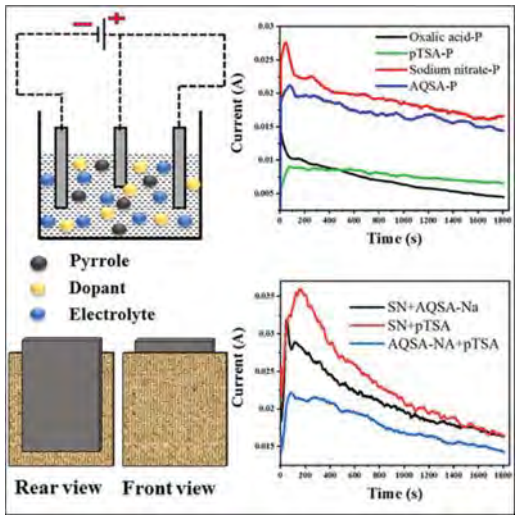

Abstract | Full text | PDF | References | Request permissions

Soft pneumatic actuator from particle reinforced silicone rubber: Simulation and experiments

Zhongming Lv, Wentao Hao, Feiyun Xiao, Pin Chen, Zhengshi Liu, Yong Wang

First Published: 13 July 2022

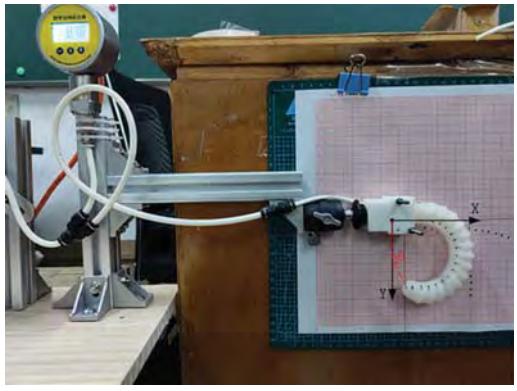

Abstract | Full text | PDF | References | Request permissions

Stretchable, conductive poly(acrylamide-*co*-maleic acid)/triethylene glycol/NaCl

double-crosslinked organohydrogel with excellent antifreezing and sensing properties

Guanfei Liu, Meiling Guo, Shishan Xue, Xi Yang, Li Wang, Chuanxia Zhao, Dong Xiang, Hui Li, Jingjuan Lai, Zhenyu Li, Yuanpeng Wu

First Published: 12 July 2022

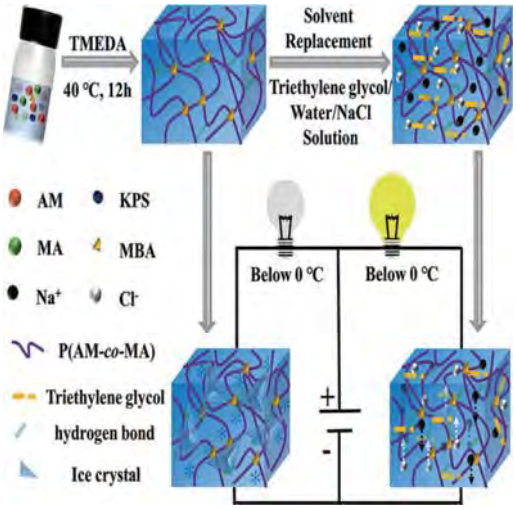

Stretchable, conductive, and antifreezing organohydrogels with double-crosslinked structure are prepared by the free radical polymerization and solvent exchange. Due to a synergistic effect between the triethylene glycol and NaCl, the organohydrogels remained flexible and conductive at −30°C, making the fabricated flexible strain sensor can work at low temperatures.

Abstract | Full text | PDF | References | Request permissions

Performance evaluation of produced biopolymers by native strains on enhanced oil recovery

Afrooz Kaboli, Arezou Jafari, Hadi Azarhava, Seyyed Mohammad Mousavi

First Published: 14 July 2022

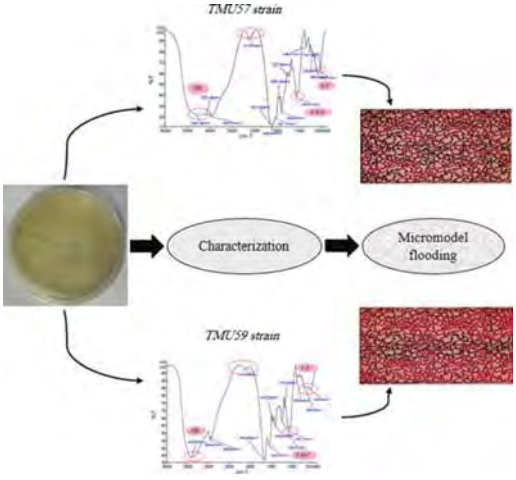

Abstract | Full text | PDF | References | Request permissions

Superhydrophobic tough hierarchical porous thermal insulation composites prepared by in situ formation of silica aerogel in collagen fiber matrix

Kaifeng Yang, Zetian Zhang, Yang Liu, Shan Li, Deyan Chen, Zhengjun Li

First Published: 13 July 2022

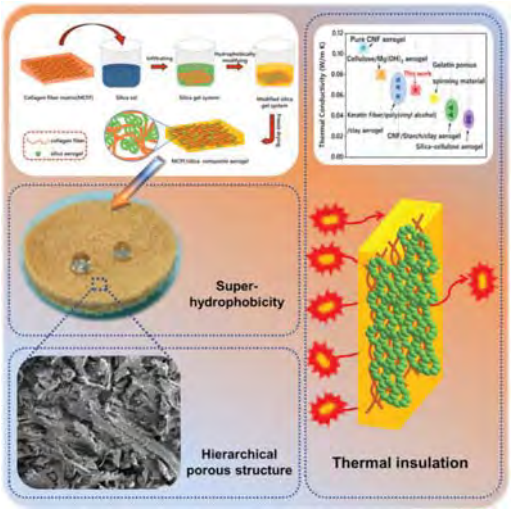

Abstract | Full text | PDF | References | Request permissions

UiO-66-NH_2 particle size effects on gas separation performance of cellulose acetate composite membranes

Zhirong Hu, Jiayu Miu, Xiong-Fei Zhang, Mingmin Jia, Jianfeng Yao

First Published: 13 July 2022

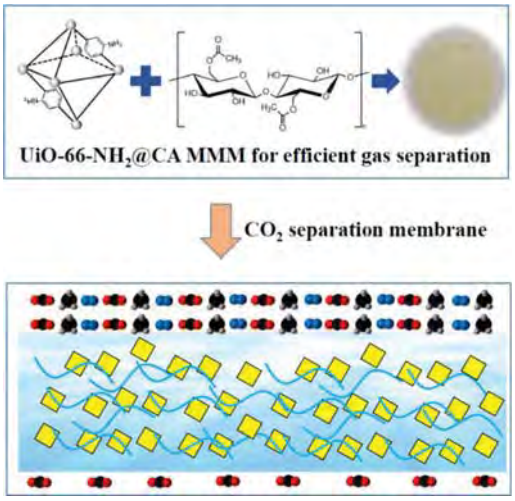

Abstract | Full text | PDF | References | Request permissions

Sign up for email alerts

Enter your email to receive alerts when new articles and issues are published.

Email address*

Enter email

Continue

Tools

Submit an Article

Browse free sample issue

Subscribe to this journal

More from this journal

- Reviews
- Professional Opportunities
- Cover Story
- Editorials
- Wiley Job Network
- Best of Wiley Polymer Journals eMagazine
- Twitter: @WileyPolymers
- Jobs

About Wiley Online Library

Privacy Policy
Terms of Use
About Cookies
Manage Cookies
Accessibility
Wiley Research DE&I Statement and Publishing Policies
Developing World Access

Help & Support

Contact Us
Training and Support
DMCA & Reporting Piracy

Opportunities

Subscription Agents
Advertisers & Corporate Partners

Connect with Wiley

The Wiley Network
Wiley Press Room

Copyright © 1999-2023 John Wiley & Sons, Inc. All rights reserved

Source details

Journal of Applied Polymer Science

Scopus coverage years: from 1959 to Present

Publisher: Wiley-Blackwell

ISSN: 0021-8995 E-ISSN: 1097-4628

Subject area: Materials Science: Polymers and Plastics | Materials Science: Materials Chemistry | Materials Science: Surfaces, Coatings and Films | Chemistry: General Chemistry

Source type: Journal

CiteScore 2021
5.0

SJR 2021
0.528

SNIP 2021
0.793

View all documents > | Set document alert | Save to source list | Source Homepage

CiteScore | CiteScore rank & trend | Scopus content coverage

CiteScore 2021

$$5.0 = \frac{26{,}004 \text{ Citations } 2018 - 2021}{5{,}189 \text{ Documents } 2018 - 2021}$$

Calculated on 05 May, 2022

CiteScoreTracker 2022

$$5.4 = \frac{31{,}046 \text{ Citations to date}}{5{,}743 \text{ Documents to date}}$$

Last updated on 05 April, 2023 • Updated monthly

CiteScore rank 2021

Category	Rank	Percentile
Materials Science Polymers and Plastics	#41/154	73rd
Materials Science Materials Chemistry	#80/298	73rd
Materials Science Surfaces, Coatings	#35/129	73rd

View CiteScore methodology > | CiteScore FAQ > | Add CiteScore to your site

About Scopus

What is Scopus

Content coverage

Scopus blog

Scopus API

Privacy matters

Language

日本語版を表示する

查看简体中文版本

查看繁體中文版本

Просмотр версии на русском языке

Customer Service

Help

Tutorials

Contact us

ELSEVIER

Terms and conditions Privacy policy

Copyright © Elsevier B.V . All rights reserved. Scopus® is a registered trademark of Elsevier B.V.
We use cookies to help provide and enhance our service and tailor content. By continuing, you agree to the use of cookies .

RELX